RECORD 2020/12

PROTEROZOIC DOLERITE DYKES IN THE WESTERN CAPRICORN OROGEN, WESTERN AUSTRALIA

by
OA Blay, MTD Wingate, SP Johnson, AM Thorne, CL Kirkland, SG Tessalina, MR Verrall and HN Cutten

John de Laeter Centre
The University Of Queensland AUSTRALIA
CSIRO
EIS Exploration Incentive Scheme
Government of Western Australia
Department of Mines, Industry Regulation and Safety
Geological Survey of Western Australia

Government of **Western Australia**
Department of **Mines, Industry Regulation and Safety**

RECORD 2020/12

PROTEROZOIC DOLERITE DYKES IN THE WESTERN CAPRICORN OROGEN, WESTERN AUSTRALIA

by
OA Blay, MTD Wingate, SP Johnson, AM Thorne[1], CL Kirkland[2], SG Tessalina[3], MR Verrall[4] and HN Cutten

1 Former manager of the Edmund and Collier Groups at Department of Mines, Industry Regulation and Safety, retired

2 Timescales of Mineral Systems Theme with the Centre for Exploration Targeting Curtin Node, School of Earth and Planetary Sciences (EPS), Curtin University, Kent Street, Bentley WA 6102

3 John de Laeter Centre for Isotope Research, Curtin University, Kent Street, Bentley WA 6102

4 CSIRO, 26 Dick Perry Avenue, Kensington WA 6155

PERTH 2020

Geological Survey of Western Australia

MINISTER FOR MINES AND PETROLEUM
Hon Bill Johnston MLA

DIRECTOR GENERAL, DEPARTMENT OF MINES, INDUSTRY REGULATION AND SAFETY
David Smith

EXECUTIVE DIRECTOR, GEOLOGICAL SURVEY AND RESOURCE STRATEGY
Jeff Haworth

REFERENCE
The recommended reference for this publication is:
Blay, OA, Johnson, SP, Wingate, MTD, Thorne, AM, Kirkland, CL, Tessalina, SG, Verrall, MR and Cutten, HN 2020, Proterozoic dolerite dykes in the western Capricorn Orogen, Western Australia, Geological Survey of Western Australia Record, 2020/12, 34p.

ISBN 978-1-74168-902-0
ISSN 2204-4345

Grid references in this publication refer to the Geocentric Datum of Australia 1994 (GDA94). Locations mentioned in the text are referenced using Map Grid Australia (MGA) coordinates, Zone 50. All locations are quoted to at least the nearest 100 m.

John de Laeter Centre

The University Of Queensland AUSTRALIA

CSIRO

EIS Exploration Incentive Scheme

U–Pb measurements were conducted using the SHRIMP II ion microprobes at the John de Laeter Centre, Curtin University, with the financial support of the Australian Research Council and Auscope NCRIS. Sm–Nd isotope analyses were conducted at the John de Laeter Centre and the University of Queensland, funded in part by the Western Australian Government Exploration Incentive Scheme (EIS). SEM imaging and analyses were conducted at the CSIRO X-ray and Electron Beam Laboratory in Perth.

Published 2020 by the Geological Survey of Western Australia
This Record is published in digital format (PDF) and is available online at <www.dmirs.wa.gov.au/GSWApublications>.

Further details of geoscience products are available from:
Information Centre
Department of Mines, Industry Regulation and Safety
100 Plain Street
EAST PERTH WESTERN AUSTRALIA 6004
Telephone: +61 8 9222 3459 Email: publications@dmirs.wa.gov.au
www.dmirs.wa.gov.au/GSWApublications

Cover image: Packing up the campsite in a claypan about 5 km south of Minilya in the southern Pilbara (photo by Olga Blay, DMIRS)

Contents

Figures

Tables

Appendices

Available with the PDF online as an accompanying digital resource

1. Whole-rock lithogeochemistry of dolerite dyke samples
2. Photomicrographs and chemical composition of individual minerals by scanning electron microscopy
3. Bivariate plots of LILE vs LOI and Zr as proxies for trace element mobility
4. Binary variation plots of selected trace element concentrations and ratios
5. Concentrations of major and trace elements in dolerite dyke and sill groups
6. Comparison of geochemical characteristics of dolerite dykes and sills

Proterozoic dolerite dykes in the western Capricorn Orogen, Western Australia

by

OA Blay, SP Johnson, MTD Wingate, AM Thorne[1], CL Kirkland[2], SG Tessalina[3], MR Verrall[4] and HN Cutten

Abstract

Field observations, petrography, geochronology, and geochemistry of dolerite dykes in the western Capricorn Orogen are employed to distinguish two dyke suites, now assigned to the Minga and Kulkatharra Dolerites, in addition to previously characterized dykes of the Mundine Well Dolerite. North-northwesterly trending Minga dykes in the westernmost part of the orogen consist of strongly altered, melanocratic dolerite of high-Fe tholeiitic affinity. Sills of Narimbunna Dolerite and dykes of the Minga Dolerite are geochemically and petrogenetically distinct. Although they have alteration and cursory geochemical similarities with Narimbunna Dolerite sills, they are not spatially associated with the sills. Together with distinctive Nd isotope compositions, our geochemical data suggest that the dykes and sills almost certainly formed independently from each other, from compositionally distinctive source rocks and through contrasting petrogenetic processes. The Minga dykes represent mantle-derived magmas, possibly with compositions resembling E-MORB, that were more or less continuously contaminated through assimilation of crustal material during emplacement. Numerous dykes are spatially associated with c. 1075 Ma Kulkatharra sills, and the two are similar mineralogically and geochemically, suggesting that the dykes were feeders for the sills. Geochemistry suggests derivation of the Kulkatharra Dolerite by extensive fractionation of either a slightly to moderately enriched mantle source or a relatively uncontaminated magma. The c. 755 Ma Mundine Well Dolerite consists mainly of north- to northeasterly trending, quartz- or olivine-dolerite dykes, which are classified as subalkaline, high-Fe to high-Mg tholeiites, derived by fractionation of a slightly to moderately enriched mantle source or contamination by evolved or old crustal material.

KEYWORDS: dolerite, dykes, geochemistry, geochronology, Sm–Nd isotopes, sills, Proterozoic

Introduction

Mafic dykes and sills are common features of Proterozoic orogens (Srivastava, 2011; Pirajno and Hoatson, 2012; Peng and Ernst, 2016). Many mafic magmatic events appear to have occurred over short time intervals, typically <5 Ma (Tarney, 2011). This makes mafic intrusive rocks important for constraining, through time, geological processes and compositional variations of magmatic source regions, particularly the subcontinental lithospheric mantle (Zhao et al., 1994; Ernst and Buchan, 2001; Pirajno and Hoatson, 2012; Peng and Ernst, 2016). Mafic dykes and sills also provide important information about the drivers of orogenesis, the nature of plate tectonic processes, and the potential role of deep mantle plumes. Because dykes and sills are typically excellent recorders of the Earth's magnetic field, integrated paleomagnetic and geochronological studies can provide important constraints on supercontinent and other geographic reconstructions (Wingate and Giddings, 2000; Wingate, 2002, 2003; Li et al., 2006; Howard et al., 2007; Wang et al., 2014; Pirajno and Santosh, 2015). Mafic dykes are also clear indicators of crustal extension and are recognized as valuable stratigraphic markers (Halls, 1982).

Recent field mapping, geochronology, geochemistry, and isotope analyses by the Geological Survey of Western Australia (GSWA) in the western Capricorn Orogen have identified two suites of dolerite dykes in addition to the Mundine Well Dolerite. These two dyke suites have geochemical compositions that initially appear consistent with a correlation with the Narimbunna and Kulkatharra Dolerites, which form extensive dolerite sills within sedimentary rocks of the Edmund and Collier Groups (Wingate, 2002; Blay et al., 2018b,c). In the case of the Kulkatharra Dolerites, U–Pb geochronology confirms that the dykes and sills are contemporaneous. However, dykes suspected to belong to the Narimbunna Dolerite, based on petrographic and geochemical similarities, have not successfully been dated. In this Record, we summarize the characteristics of the newly investigated dolerite dykes and of previously sampled dykes and sills of the Narimbunna, Kulkatharra and Mundine Well Dolerites. We assess the

1 Former manager of the Edmund and Collier Groups at Department of Mines, Industry Regulation and Safety, retired

2 Timescales of Mineral Systems Theme with the Centre for Exploration Targeting Curtin Node, School of Earth and Planetary Sciences (EPS), Curtin University, Kent Street, Bentley WA 6102

3 John de Laeter Centre for Isotope Research, Curtin University, Kent Street, Bentley WA 6102

4 CSIRO, 26 Dick Perry Avenue, Kensington WA 6155

validity of the potential correlation between the newly investigated dolerite dykes with sills of Narimbunna Dolerite, discuss the likely source regions for these regional dolerite suites, and describe some spatial variations in the compositions of the Kulkatharra Dolerite that may have implications for regional tectonic evolution.

Geological setting

The Capricorn Orogen is a Proterozoic orogenic belt, about 1000 km long and 500 km wide (Figs 1, 2), located between the Archean Pilbara and Yilgarn Cratons in Western Australia (Cawood and Tyler, 2004; Johnson et al., 2013). The orogen records nearly two billion years of orogenic activity, including continental collision and subsequent intraplate reactivation, and is the product of at least seven major orogenic events. The 2215–2145 Ma Ophthalmia and 2005–1950 Ma Glenburgh Orogenies (Rasmussen et al., 2005; Johnson et al., 2010, 2011) record the punctuated assembly of the Pilbara and Yilgarn Cratons with the Glenburgh Terrane to form the West Australian Craton.

Following craton assembly, the orogen was reworked during several intraplate events, including the 1820–1770 Ma Capricorn Orogeny, the 1680–1620 Ma Mangaroon Orogeny, the 1321–1171 Ma Mutherbukin Tectonic Event, the 1030–955 Ma Edmundian Orogeny, the 931–794 Ma Kuparr Tectonic Event, and the c. 570 Ma Mulka Tectonic Event (Cawood and Tyler, 2004; Sheppard, 2004; Sheppard et al., 2007, 2010; Johnson et al., 2013, 2017a,b; Korhonen et al., 2017; Cutten and Johnson, 2018; Piechocka et al., 2018; Olierook et al., 2019). The two oldest reworking events were accompanied by voluminous granite magmatism, with little to no evidence for mafic magmatism (Johnson et al., 2017a,b). Following the Mangaroon Orogeny, the orogen became more rigid in character, similar to that of the bounding Archean Yilgarn and Pilbara Cratons (Johnson et al., 2017a,b). This allowed the emplacement of abundant mafic dykes and sills into the shallow crust (Wingate, 2002, 2003; Wingate et al., 2004; Morris and Pirajno, 2005), and the formation of the thick intracontinental sedimentary Edmund and Collier Basins (Martin and Thorne, 2004; Martin et al., 2008; Cutten et al., 2016). Basin formation was associated with only minimal felsic magmatism (e.g. Wingate et al., 2012).

Low-grade sedimentary rocks of the 1679–1455 Ma Edmund Basin were intruded by dolerite sills of the 1514–1505 Ma Waldburg Dolerite, the 1465–1450 Ma Narimbunna Dolerite, and the 1083–1075 Ma Kulkatharra Dolerite, whereas the overlying >1083–1067 Ma Collier Basin was intruded by the Kulkatharra Dolerite (Wingate, 2002; Martin et al., 2005; Morris and Pirajno, 2005; Martin et al., 2007; Thorne and Martin, 2007; Blay et al., 2018a–c; Blay et al., 2020). The Kulkatharra Dolerite is a component of the c. 1075 Ma Warakurna Large Igneous Province, which extended mainly as sills and dykes over at least 2×10^6 km^2 in central and western Australia (Wingate et al., 2004; Smithies et al., 2015; Wingate, 2017a; Howard et al., 2019). In contrast, the Waldburg and Narimbunna Dolerites are not known to occur outside the Edmund Basin.

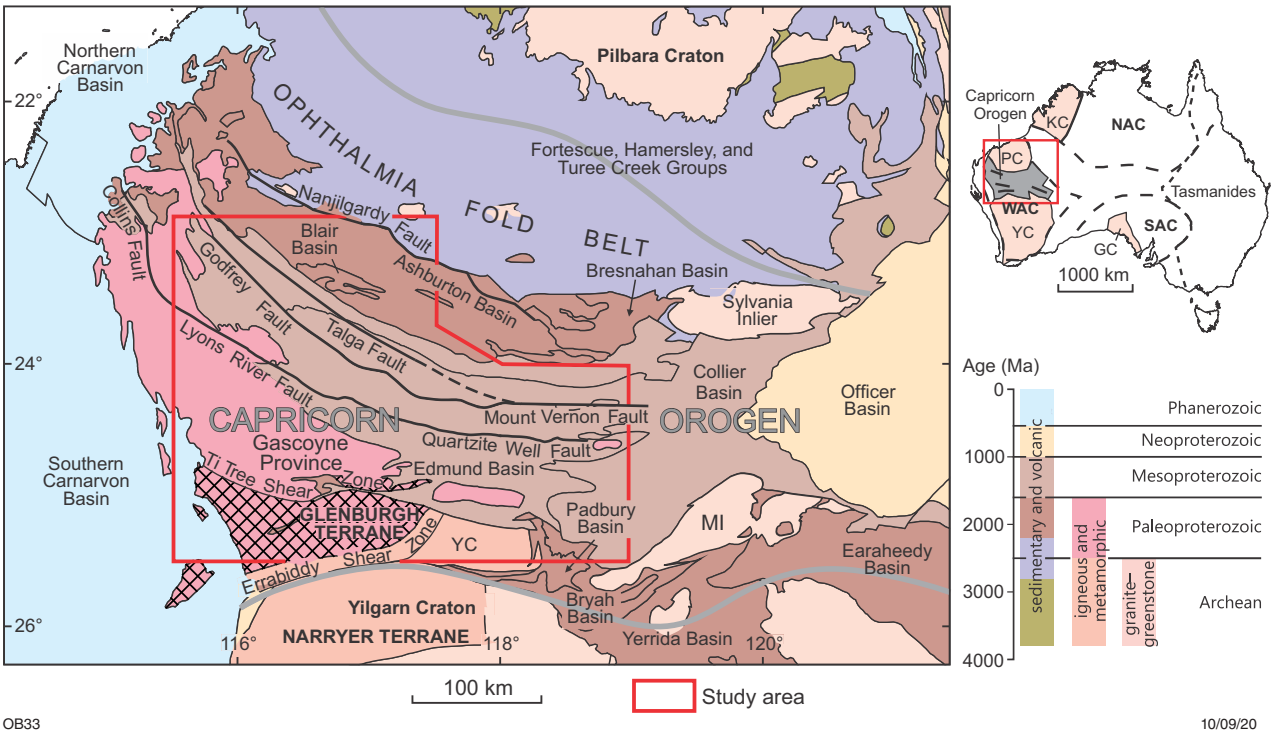

Figure 1. **Major geological elements of the Capricorn Orogen, showing surrounding cratons and basins, and the location of the study area (modified after Johnson et al., 2013). Abbreviations: GC, Gawler Craton; KC, Kimberley Craton; MI, Marymia Inlier; NAC, North Australian Craton; PC, Pilbara Craton; SAC, South Australian Craton; WAC, West Australian Craton; YC, Yilgarn Craton**

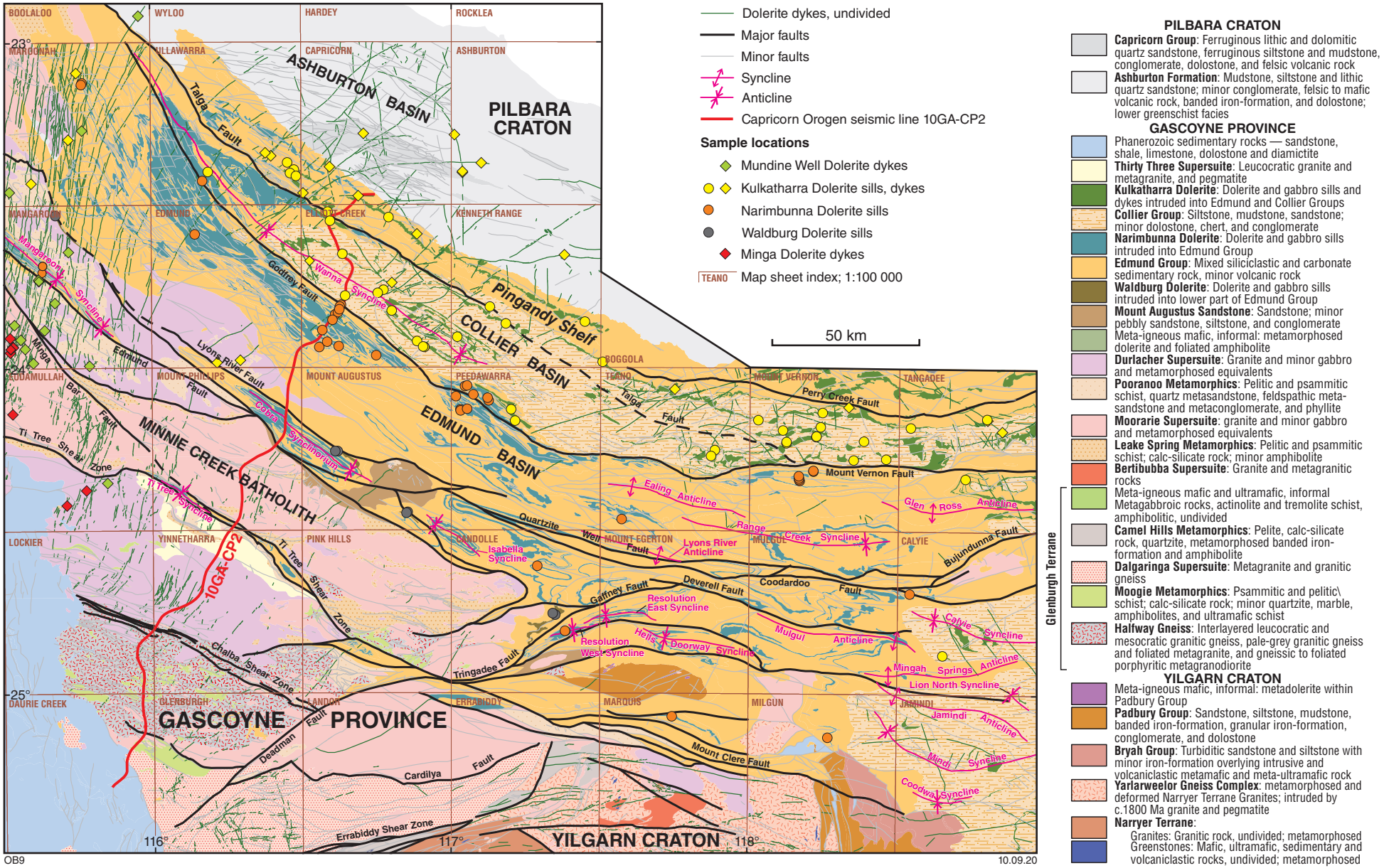

Figure 2. Geology and principal structural elements of the western Capricorn Orogen (modified after Cutten et al., 2016) showing dolerite dyke and sill sample locations. A complete list of dyke samples, coordinates, and host rocks is provided in Appendix 1

The Capricorn Orogen is intruded by numerous mafic dykes and sills (Fig. 2). The dykes exhibit a wide variety of orientations and crosscutting relationships. The most prominent dyke swarm is the c. 755 Ma Mundine Well Dolerite (Hickman and Lipple, 1975; Wingate and Giddings, 2000; Li et al., 2006). The Mundine Well dykes are concentrated in the western Capricorn Orogen, where they trend mainly north to north-northeast, and also extend northeastwards across the Pilbara Craton. However, crosscutting relationships, orientations, and magnetic characteristics indicate that there are additional suites of mafic dykes within the western Capricorn Orogen, including some that may have acted as feeders to dolerite sills of the Narimbunna and Kulkatharra Dolerites (Daniels, 1968; Muhling and Brakel, 1985; Wingate, 2002; Martin et al., 2005; Morris and Pirajno, 2005; Blay et al., 2018c). For example, Wingate, 2002 described a north-northeasterly trending dolerite dyke intruded into the c. 2450 Ma Woongarra Rhyolite of the upper Hamersley Group (Wyloo 1: 100 000 map sheet). The dyke yielded paleomagnetic directions (DAD Evans, written comm., 2000) that are similar to primary paleomagnetic directions obtained from sills of the c. 1075 Ma Kulkatharra Dolerite, indicating that the dyke is similar in age to the sills (Wingate, 2002).

Dolerite dykes were emplaced into both Neoarchean–Paleoproterozoic medium- to high-grade basement rocks and Paleoproterozoic–Mesoproterozoic low-grade metasedimentary cover rocks (Fig. 2, Appendix 1). There are also several arcuate dykes (not discussed in this Record) in the northern Capricorn Orogen that cut Paleoproterozoic to Mesoproterozoic metasedimentary rocks of the Ashburton, Blair, and Edmund Basins (Fig. 3). Most dykes exhibit moderate to strong magnetic remanence and are readily identified in aeromagnetic images (Figs 3, 4), except in areas where they are aligned parallel to the structural grain of the orogen (Figs 4, 5). Dykes are most abundant in the western Capricorn Orogen, where most strike north-northeast, intruding mainly metamorphic and granitic rocks of the northern Gascoyne Province and sedimentary rocks of the lower Edmund Group (Thorne, 2016b; Fig. 2). Dykes of the c. 755 Ma Mundine Well Dolerite (Wingate and Giddings, 2000) cut across all older rocks.

Analytical methods

Petrography

Polished thin sections were made of samples collected from 42 dyke outcrops during fieldwork in 2010–13. Together with 11 additional samples from the GSWA collection, the sections were examined using an Olympus TH4-200 optical microscope. To aid mineral identification, 198 semiquantitative compositional analyses were conducted on seven polished thin sections, using a Philips (FEI) XL40 scanning electron microscope (SEM) fitted with an energy dispersive X-ray spectrometer (EDS) and a Zeiss UltraPlus field emission SEM at the X-ray and Electron Beam Laboratory, CSIRO, in Perth, Western Australia.

Geochronology

Sensitive High-Resolution Ion Microprobe (SHRIMP) U–Pb zircon and baddeleyite crystallization ages have been reported previously for Narimbunna and Kulkatharra sills, and the Mundine Well Dolerite (Wingate and Giddings, 2000; Blay et al., 2018c). New SHRIMP U–Pb zircon and baddeleyite results are included in this Record for two Kulkatharra dykes and one Mundine Well dyke. Geochronology was conducted using SHRIMP instruments in the John de Laeter Centre at Curtin University in Perth. Details of each sample, including analytical parameters, are included in each cited Geochronology Record, and procedures are similar to those described by Wingate and Lu, 2018. All isotopic ages discussed in this Record are based on $^{207}Pb^*/^{206}Pb^*$ ratios (Pb*, radiogenic Pb) and quoted with 95% confidence intervals.

Geochemistry

Whole-rock major and trace element geochemical analyses were conducted on 49 samples of fine- to medium-grained dolerite. All results are published online (GSWA, 2020), and some have been interpreted previously (Morris and Pirajno, 2005). Weathered surfaces and veinlets were removed and the samples were washed, dried, crushed, and milled to a very fine powder (90% <75 microns). A 50 g split was used for geochemical analysis by standard X-ray fluorescence (XRF) and inductively coupled plasma mass spectrometric (ICPMS) techniques (Morris and Pirajno, 2005). Trace element analyses were conducted by ICPMS at the Ultratrace Laboratory of Bureau Veritas Australia Pty Ltd, Western Australia (Appendix 1). Fourteen of the 49 dolerite samples were analysed for platinum group elements (PGE) and Au, with detection limits of 0.1 ppb and 0.1 ppb, respectively, by nickel sulfide fire assay. Results for major element oxides, trace elements, and loss on ignition (LOI) are tabulated in Appendix 1.

Isotope analyses

Sm–Nd isotope compositions of 16 dyke samples were measured (laboratory details are in Table 2) on separate splits of the same powders used for whole-rock geochemistry, and were determined by isotope dilution thermal ionization mass spectrometry (IDTIMS) or laser ablation multicollector inductively coupled plasma mass spectrometry (LA-MC-ICPMS), (e.g. Stern, 2001; Morris and Pirajno, 2005; Kirkland et al., 2011). Two-stage Sm–Nd model ages (T_{DM}^2) were calculated using the depleted mantle model of Goldstein et al. (1984):

$$^{147}Sm/^{144}Nd = 0.2136,\ ^{143}Nd/^{144}Nd = 0.513163$$

and an average crustal $^{147}Sm/^{144}Nd$ of 0.11. Present-day chondritic uniform reservoir (CHUR) values are from Bouvier et al., 2008 and Champion and Huston, 2016:

$$^{147}Sm/^{144}Nd = 0.512630 \text{ and } ^{147}Sm/^{144}Nd = 0.1960$$

and a decay constant of ^{147}Sm = 6.54 x 10–12 (Lugmair and Marti, 1978).

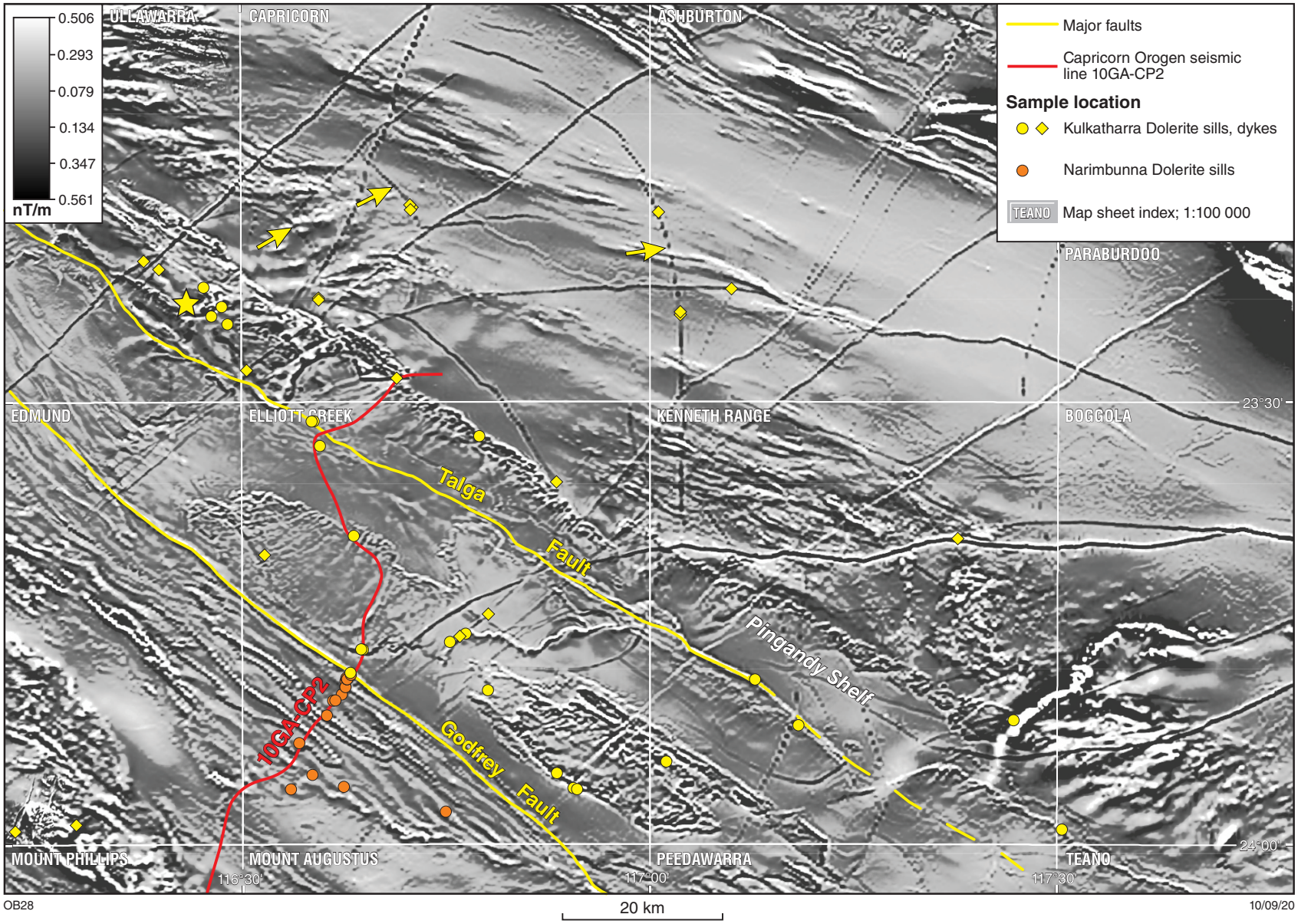

Figure 3. Magnetic image 1VD–TMI of the north–central project area, showing arcuate Kulkatharra Dolerite dykes (arrows) that are centred approximately on a high-intensity magnetic anomaly (star) and closely coincide with a Kulkatharra? Dolerite sill

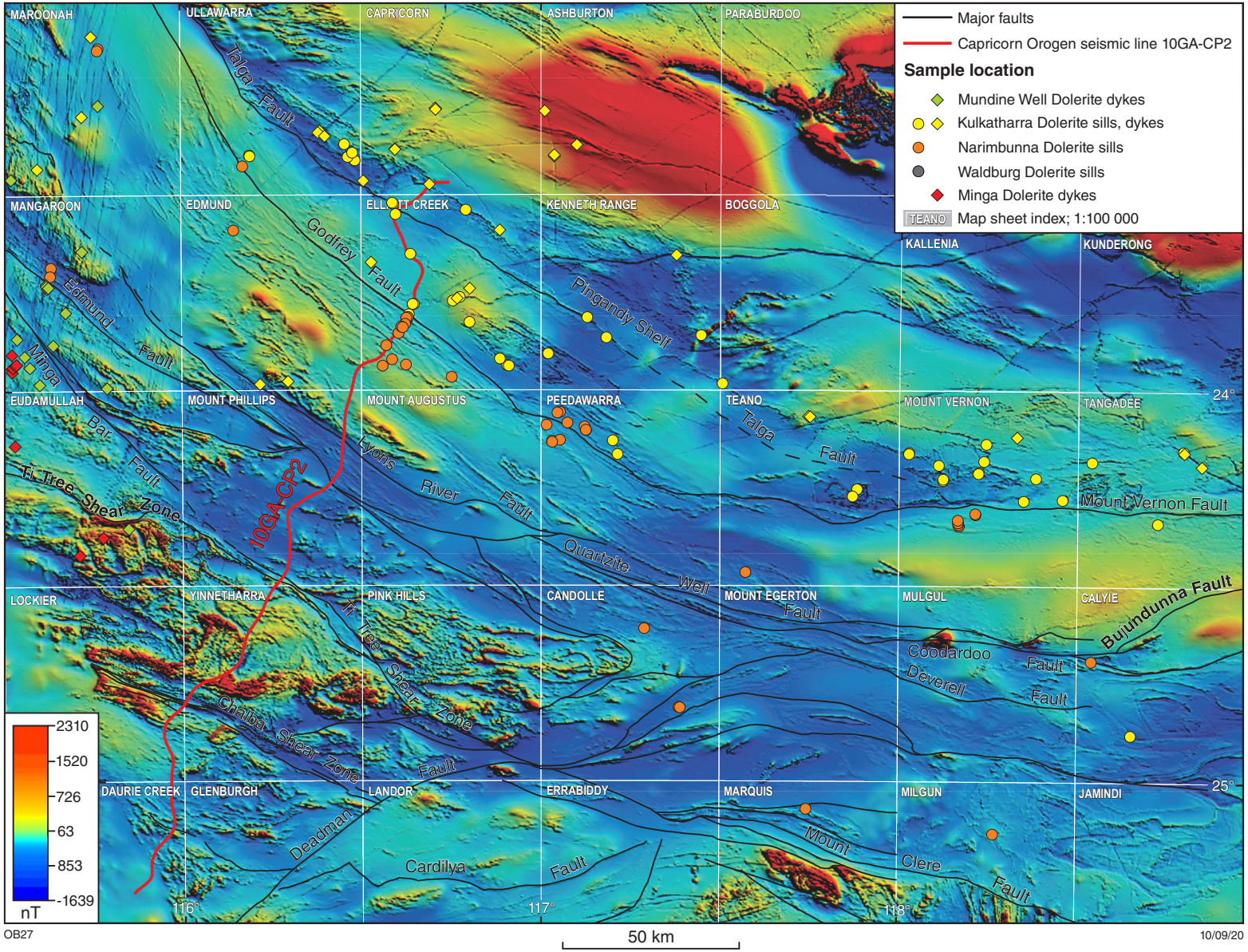

Figure 4. Total magnetic intensity image (80 m pixel resolution) of the western Capricorn Orogen, showing major faults, and sample locations in dolerite dykes and sills

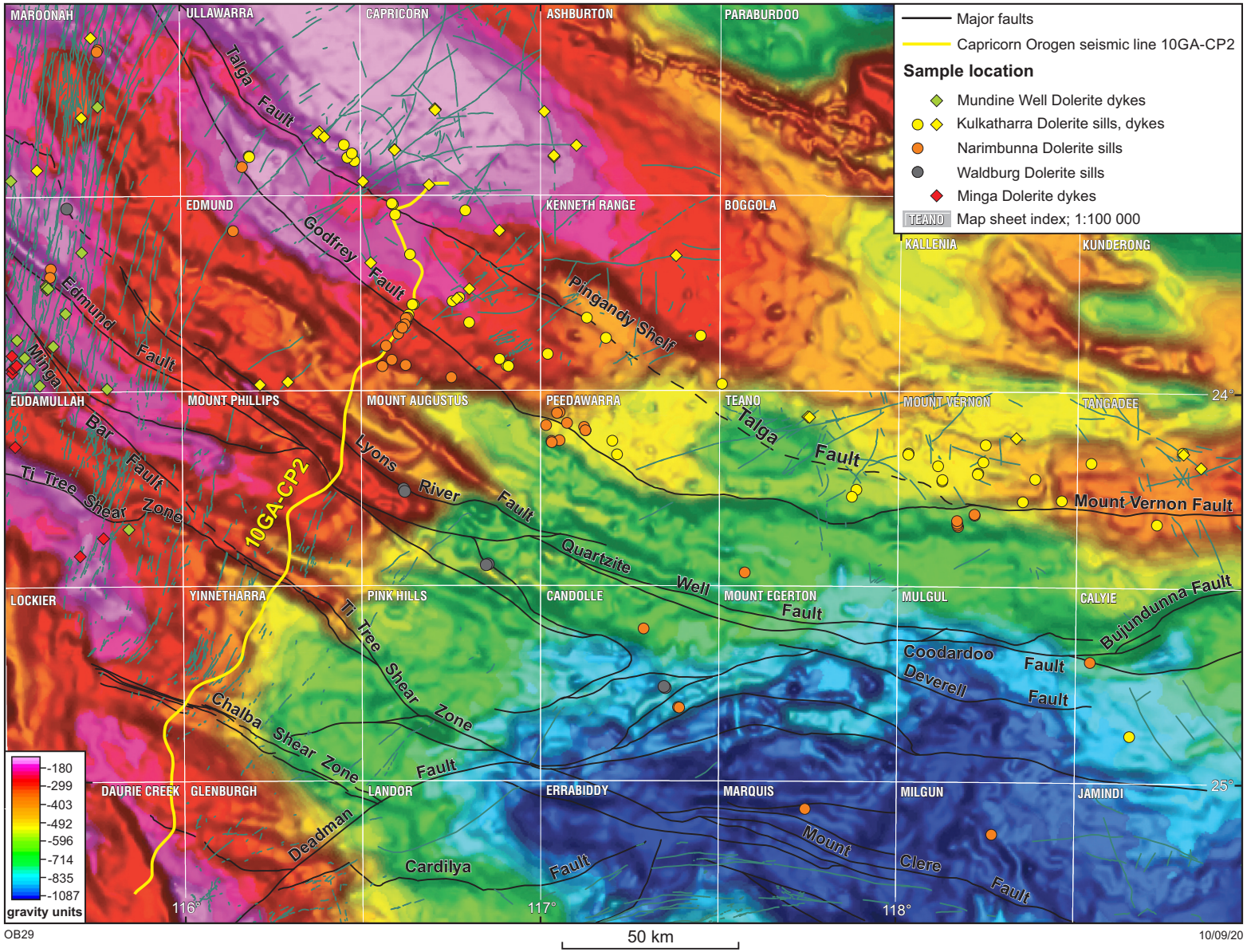

Figure 5. Shaded Bouguer gravity anomaly image of the western Capricorn Orogen, showing major faults, and sample locations in dolerite dykes and sills. Gravity units are µm/s2 (10 µm/s2 = 1 mGal)

Minga Dolerite dykes

Field observations

Dykes with geochemical similarities with the 1465–1450 Ma Narimbunna Dolerite trend mainly north-northwest, and to a lesser extent north-northeast, in the western Capricorn Orogen on Mangaroon and Eudamullah (Fig. 2). Referred to here as the Minga Dolerite, these dykes intrude metamorphosed Paleoproterozoic metasedimentary and meta-igneous rocks of the central Gascoyne Province, including the 1758–1682 Ma Pooranoo Metamorphics (Sheppard and Johnson, 2018), and the 1817–1773 Ma Moorarie and 1689–1619 Ma Durlacher Supersuites (Sheppard et al., 2018a,b; Sheppard and Johnson, 2018). Martin et al., 2005 noted abundant north-northwesterly trending dolerite dykes within the Minnie Creek batholith on Mount Phillips and Pink Hills (Fig. 2). The Minga dykes are not spatially associated with sills of known Narimbunna Dolerite, which outcrop farther to the east. However, all of the Minga dykes and most Narimbunna Dolerite sills were emplaced south-southwest of the Godfrey Fault which, together with the Talga and Mount Vernon Faults, forms a major crustal shear zone (Johnson et al., 2013).

Exposed typically as small, low, rubbly outcrops, Minga dykes are up to 70 m wide, with strike lengths up to 25 km. They are difficult to identify in aeromagnetic images because they typically parallel the regional structural architecture and magnetic grain (Fig. 4). The Minga dykes are typically highly altered and greenish, features that distinguish them from the younger Kulkatharra and Mundine Well dyke suites. Away from chilled margins, the dykes are typically equigranular, although they can vary from fine grained to very coarse grained. The rocks have been metamorphosed under low- to medium-grade conditions, although primary subophitic to intergranular textures are generally well preserved (Fig. 6a). Some dykes contain inclusions of granitic rock aligned parallel to dyke margins (e.g. SXSMAN6120, 349379E 7355420N). Where they are crosscut by Mundine Well dykes, Minga dykes are locally contact metamorphosed (e.g. SXSMAN6121, 349260E 7355550N), although they are not significantly offset (Wingate and Giddings, 2000; Martin et al., 2005), e.g. SXSMAN6119, 349730E 7356210N.

Petrography

Minga dykes are distinctive petrographically, and primary minerals include plagioclase (andesine–labradorite) and clinopyroxene (augite), with subordinate quartz, alkali feldspar, and opaque minerals (magnetite, ilmenite). Granophyre (5–15%) forms interstitial patches. Accessory minerals include chlorite, apatite, titanite, zircon and sulfide minerals (pyrite, chalcopyrite, bornite). However, the Minga dykes are extensively altered, and secondary minerals include hornblende, greenish-blue amphibole, clinozoisite–epidote, and minor biotite, sericite, and iron hydroxide minerals. The chemical compositions of selected minerals are detailed in Appendix 2.

Plagioclase is subhedral to anhedral, and typically intergrown with altered pyroxene and anhedral opaque minerals. Clinozoisite–epidote and minor sericite are common alteration products of plagioclase (Fig. 6c; Appendix 2 Fig. 2.10a–c). Plagioclase is clouded by exsolved micron-scale, acicular magnetite inclusions (Fig. 6a, Appendix 2), reflecting crystallization at high pressures and temperatures (Halls and Zhang, 1995). Minor tension fractures commonly transect plagioclase grains and are more distinct in larger crystals.

Clinopyroxene is preserved as rare relict cores surrounded by brown rims of mainly hornblende and is generally strongly fractured (Fig. 6d). The hornblende is typically overgrown by strongly pleochroic greenish-blue amphibole (Fig. 6b,e; Appendix 2 Fig. 2.10a). SEM analyses indicate that the hornblende rims are mineralogically complex, with compositions that include ferromagnesian hornblende, ferrohornblende, tremolite–actinolite minerals, and minor magnesiohornblende (Appendix 2). The greenish-blue amphibole also occurs along fractures in plagioclase, and SEM analysis indicates a complex mixture of Na-rich calcic amphiboles, including edenite, Fe-edenite, and mineral phases such as ferrotschermakite, aluminoferrotshermakite, and tschermakite series (Appendix 2).

Some mineral compositions may reflect postmagmatic metasomatism by alkali-rich fluids. The greenish-blue amphibole is typically intergrown with biotite (Fig. 6e), and associated with fine-grained prismatic and/or bladed clinozoisite–epidote crystals (Fig. 6e; Appendix 2 Fig. 2.10b). Interstitial quartz–biotite and granophyre patches are commonly enriched in acicular apatite crystals up to 2.5 mm long. Biotite flakes are locally overgrown by titanite aggregates typically surrounded by pleochroic haloes. Very fine-grained sulfide minerals such as chalcopyrite and bornite are commonly associated with tremolite–actinolite minerals, hornblende, and greenish-blue amphibole (Fig. 7a,b; Appendix 2 Figs 2.5 – 2.9), or are marginal to, or overgrow, opaque minerals (Fig. 8). Opaque minerals are mainly anhedral ilmenite and titanomagnetite up to 3.5 mm in size, exhibit exsolution lamellae, and are locally overgrown by pyrite (Fig. 8a,b). Some ilmenite and magnetite crystals contain trace amounts of Mn (Appendix 2 Figs 2.1, 2.9, 2.10).

Geochronology

No Minga dykes have been dated directly. Samples processed by GSWA for SHRIMP U–Pb geochronology failed to yield dateable minerals such as zircon, baddeleyite, and zirconolite, despite Zr concentrations up to 231 ppm in some samples (Appendix 1). This suggests that Zr in these rocks resides in other minerals, such as titanite, amphibole, clinopyroxene, ilmenite, or magnetite (e.g. Bingen et al., 2001; Bea et al., 2006).

Geochemistry

Minga dykes have distinctive alteration characteristics and geochemical compositions, in terms of their major and trace element concentrations (Table 1; Appendix 1).

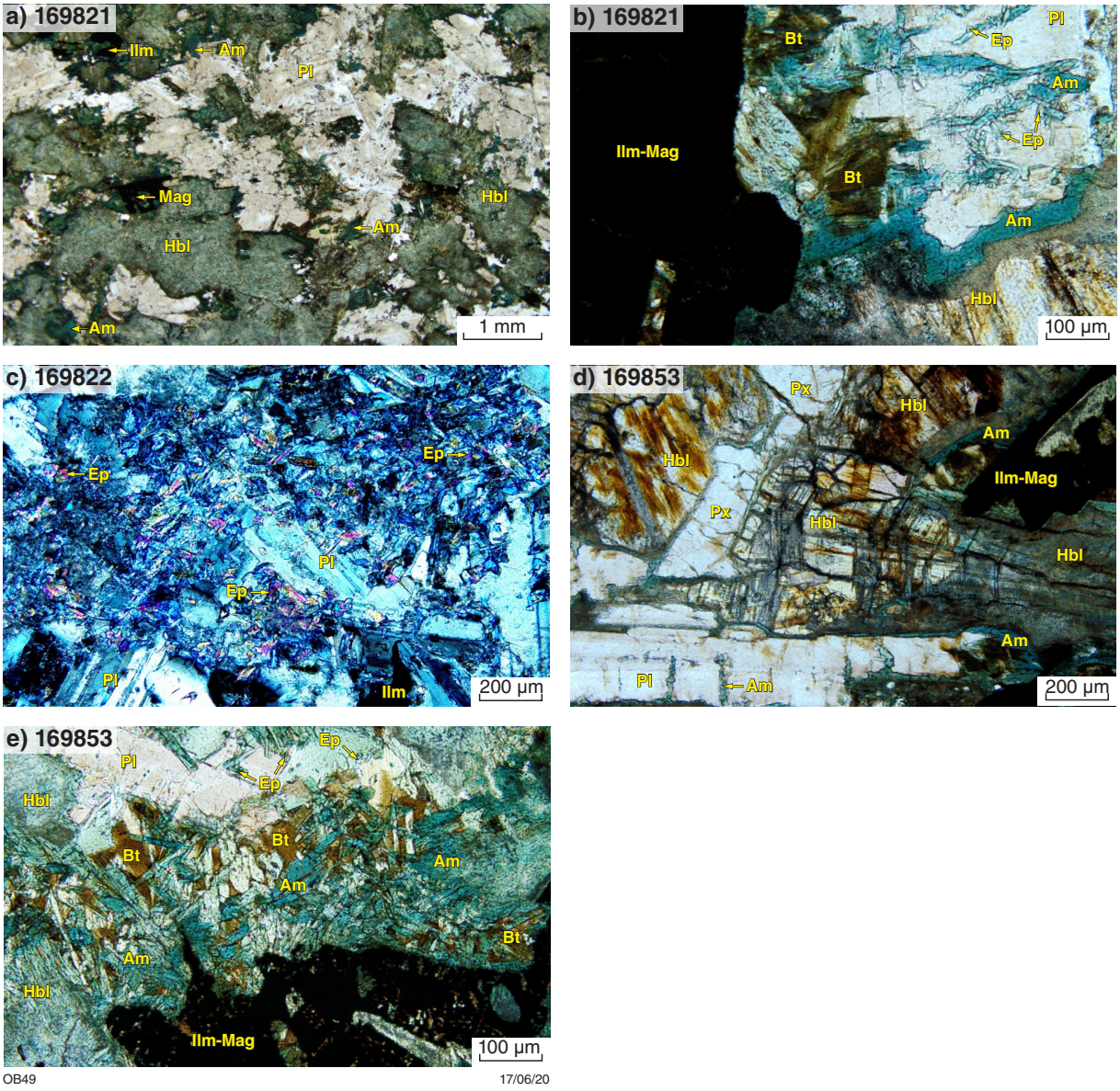

Figure 6. **Photomicrographs of Minga Dolerite dyke samples. Sample GSWA 169821 (plane-polarized light): a) coarse-grained subophitic metadolerite with clouded plagioclase (Pl) dusted with minute inclusions; b) colourless to brown hornblende rimmed by strongly pleochroic pale yellow–brown to dark blue amphibole (Am) and ?secondary biotite (Bt). Sample GSWA 169822 (cross-polarized light); c) short to elongate prisms and fine-grained aggregates of clinozoisite–epidote minerals (Ep) overgrowing plagioclase laths. Sample GSWA 169853 (plane-polarized light); d) pyroxene (Px) crystals replaced by anhedral fibrous to prismatic brownish hornblende (Hbl), either as intergrown chaotically oriented flakes and/or pseudomorphs that retain the crystallographic orientation of the primary pyroxene preserved as cores within brownish–green hornblende; e) aqua-blue amphibole, biotite, and fine prismatic clinozoisite–epidote minerals rimming 'dirty' hornblende and/or developing along fracture planes in clouded plagioclase. Other abbreviation: Ilm–Mag, ilmenite–magnetite**

Table 1. Major oxides and trace elements in dolerite dyke samples

	Minga Dolerite dykes		*Kulkatharra Dolerite dykes*		*Mundine Well Dolerite dykes*	
	Average	*Range*	*Average*	*Range*	*Average*	*Range*
Oxides	*Percentage (wt%)*					
SiO_2	49.80	48.54 – 50.50	49.24	47.30 – 51.80	49.94	47.39 – 52.12
TiO_2	2.19	1.28 – 2.65	2.77	1.62 – 4.32	1.75	0.67 – 2.80
Al_2O_3	12.90	12.07 – 13.70	12.83	11.42 – 14.00	14.39	13.10 – 15.60
$*Fe_2O_3^T$	16.09	13.67 – 17.77	15.88	12.47 – 20.01	12.84	8.97 – 15.62
MnO	0.23	0.21 – 0.25	0.20	0.06 – 0.24	0.19	0.15 – 0.22
MgO	5.35	4.18 – 6.61	5.20	4.25 – 6.96	6.78	3.37 – 12.60
CaO	9.61	8.79 – 10.90	8.45	3.70 – 10.35	10.00	8.49 – 11.24
Na_2O	2.29	2.12 – 2.51	2.39	1.79 – 2.99	2.11	1.35 – 2.83
K_2O	0.63	0.35 – 0.93	0.99	0.36 – 1.62	0.89	0.62 – 1.60
P_2O_5	0.24	0.12 – 0.35	0.31	0.18 – 0.54	0.19	0.06 – 0.34
Elements	*Parts per million (ppm)*					
Cr	81	36–120	86	36–160	184	40–514
Ni	57	39–78	69	48–127	99	40–361
V	351	251–447	415	234–726	261	139–340
Pb	6.9	3.0 – 9.0	9.1	1.0 – 14.0	6.3	4.0 – 11.0
Cu	212	125–330	184	111–388	109	70–156
La	15.92	8.90 – 23.65	29.45	19.30 – 62.00	16.37	8.67 – 25.60
Ce	37.93	21.10 – 55.00	65.03	42.10 – 121.0	37.07	19.05 – 57.60
Pr	5.20	2.96 – 7.41	8.4	5.32 – 15.35	4.86	2.29 – 7.81
Nd	23.29	11.90 – 33.72	34.53	23.10 – 55.00	19.63	9.77 – 29.50
Sm	6.19	3.23 – 8.36	8.22	5.39 – 11.40	4.47	2.35 – 6.81
Eu	1.97	1.14 – 2.58	2.40	1.59 – 3.22	1.51	0.80 – 2.32
Gd	6.82	4.10 – 9.23	8.69	6.02 – 11.05	4.81	2.39 – 7.36
Tb	1.08	0.66 – 1.46	1.35	0.90 – 1.69	0.77	0.39 – 1.12
Dy	6.61	4.03 – 8.45	7.66	5.09 – 9.49	4.41	2.09 – 6.44
Ho	1.4	0.86 – 1.88	1.54	1.02 – 1.94	0.92	0.46 – 1.30
Er	3.80	2.43 – 5.09	4.07	2.66 – 5.22	2.54	1.26 – 3.56
Yb	3.50	2.40 – 4.69	3.56	2.16 – 4.88	2.33	1.06 – 3.30
Lu	0.51	0.34 – 0.66	0.51	0.28 – 0.68	0.34	0.16 – 0.47
Y	39.0	24.5 – 52.7	42.9	29.8 – 57.4	25.7	12.1 – 37.2
Zr	165	86 – 231	229	156–320	127	57–201
Nb	11.5	5.8 – 15.5	18.5	8.7 – 33.0	11.0	3.3 – 17.2
Hf	4.41	2.20 – 6.50	6.10	4.00 – 9.00	3.37	1.39 – 5.20
Th	2.18	1.05 – 3.39	5.58	2.18 – 9.14	3.37	1.28 – 6.57
U	0.46	0.21 – 0.69	0.84	0.54 – 1.32	0.65	0.41 – 1.03
Ti	13 155	7674–15 911	16615	9712–25 899	10482	4041–16 787
Ta	0.79	0.50 – 1.10	1.23	0.70 – 2.60	0.85	0.23 – 1.40
Sc	40.0	37.0 – 43.0	30.9	25.0 – 36.0	32.3	21.0 – 38.0
Ga	20.2	17.2 – 23.1	23.7	20.5 – 26.3	18.9	14.4 – 23.6

NOTE: *All Fe as Fe_2O_3

Table 2. Sm–Nd isotope analyses of whole-rock dolerite dyke and sill samples

Sample ID	Age (Ma)	Sm (ppm)	Nd (ppm)	$^{147}Sm/^{144}Nd$	$^{143}Nd/^{144}Nd$ measured	2σ	$^{143}Nd/^{144}Nd_{(i)}$	$\varepsilon_{Nd(i)}$	T_{DM}^{2} (Ga)	Method	Lab.
Mundine Well Dolerite dykes											
178711	755	2.3	10.2	0.137784	0.512235	0.000006	0.511553	-2.09	1.57	IDTIMS	UQ
178715	755	6.3	25.9	0.149237	0.512358	0.000014	0.511620	-0.78	1.47	MC-ICPMS	JdLC
178725	755	3.7	16.0	0.142145	0.512190	0.000032	0.511486	-3.39	1.67	MC-ICPMS	JdLC
178731	755	4.5	18.7	0.147736	0.512425	0.000007	0.511694	0.66	1.36	MC-ICPMS	JdLC
178745	755	3.1	13.4	0.140109	0.512202	0.000005	0.511508	-2.96	1.63	IDTIMS	UQ
178767	755	5.1	22.4	0.141382	0.512330	0.000010	0.511630	-0.58	1.46	MC-ICPMS	JdLC
169819	755	2.4	10.3	0.146996	0.511891	0.000006	0.511163	-9.70	2.14	MC-ICPMS	JdLC
Kulkatharra Dolerite dykes											
152933	1075	6.7	27.7	0.144000	0.512305	0.000009	0.511289	0.82	1.62	MC-ICPMS	SU
169829	1075	9.1	37.3	0.150967	0.512114	0.000004	0.511049	-3.87	1.97	MC-ICPMS	JdLC
169854	1075	8.2	34.3	0.144666	0.511817	0.000008	0.510796	-8.82	2.34	MC-ICPMS	JdLC
169855	1075	9.0	39.4	0.140929	0.512219	0.000003	0.511225	-0.44	1.71	MC-ICPMS	JdLC
169856	1075	8.7	38.2	0.141122	0.512223	0.000005	0.511227	-0.39	1.71	MC-ICPMS	JdLC
169858	1075	9.4	41.3	0.140107	0.512200	0.000003	0.511212	-0.69	1.73	MC-ICPMS	JdLC
169825	1075	9.2	40.9	0.139413	0.512206	0.000005	0.511222	-0.48	1.71	MC-ICPMS	JdLC
169827	1075	6.9	29.0	0.146929	0.512292	0.000012	0.511255	0.16	1.67	MC-ICPMS	JdLC
169859	1075	6.1	28.4	0.131771	0.511952	0.000007	0.511022	-4.41	2.01	MC-ICPMS	JdLC
169860	1075	7.1	30.1	0.145595	0.512288	0.000009	0.511261	0.26	1.66	MC-ICPMS	JdLC
189201	1075	6.4	26.5	0.145833	0.512269	0.000005	0.511240	-0.14	1.69	IDTIMS	UQ
Kulkatharra Dolerite sills											
127277	1070	4.7	19.4	0.146271	0.512176	0.000004	0.511149	-2.05	1.83	IDTIMS	UQ
127298	**1067**	5.3	23.7	0.138432	0.512134	0.000007	0.511165	-1.82	1.81	MC-ICPMS	CU
180705	**1068**	5.4	23.8	0.140842	0.512145	0.000006	0.511158	-1.92	1.82	MC-ICPMS	CU
152927	1070	6.2	26.3	0.145274	0.512413	0.000071	0.511392	2.71	1.47	MC-ICPMS	CU
152927	1070	6.5	26.6	0.147000	0.512309	0.000012	0.511277	0.45	1.64	MC-ICPMS	SU
152928	1070	6.6	28.7	0.141465	0.512214	0.000008	0.511221	-0.64	1.72	MC-ICPMS	CU
152928	1070	6.8	28.6	0.142000	0.512220	0.000012	0.511223	-0.60	1.72	MC-ICPMS	SU
156543	1070	5.3	22.3	0.146268	0.512295	0.000009	0.511268	0.29	1.65	MC-ICPMS	CU
156723	1070	5.5	24.1	0.138000	0.512100	0.000023	0.511131	-2.40	1.85	MC-ICPMS	SU
156681	**1084**	6.1	23.6	0.159552	0.512385	0.000009	0.511250	0.28	1.66	MC-ICPMS	CU
160185	1070	6.8	28.6	0.143000	0.512199	0.000011	0.511195	-1.15	1.76	MC-ICPMS	SU
160195	**1071**	5.7	24.2	0.140970	0.512159	0.000006	0.511168	-1.65	1.80	IDTIMS	UQ
160195	1070	5.6	24.5	0.138000	0.512104	0.000010	0.511135	-2.32	1.85	MC-ICPMS	SU
180706	1070	5.1	23.6	0.129000	0.512178	0.000019	0.511272	0.36	1.65	MC-ICPMS	SU

Table 2. continued

Sample ID	Age (Ma)	Sm (ppm)	Nd (ppm)	$^{147}Sm/^{144}Nd$	$^{143}Nd/^{144}Nd$ measured	2σ	$^{143}Nd/^{144}Nd_{(i)}$	$\varepsilon_{Nd(i)}$	T_{DM}^2 (Ga)	Method	Lab.
Narimbunna Dolerite sills											
127297	1465	5.3	22.1	0.145000	0.511969	0.000014	0.510573	-3.33	2.25	MC-ICPMS	SU
127292	1465	4.2	16.9	0.148630	0.512045	0.000005	0.510614	-2.52	2.19	IDTIMS	UQ
148983	1465	4.6	21.7	0.131828	0.511752	0.000006	0.510482	-5.10	2.38	MC-ICPMS	CU
143450	**1452**	3.8	16.2	0.143130	0.512019	0.000005	0.510653	-2.09	2.15	IDTIMS	UR
156684	1465	5.3	23.1	0.138622	0.511907	0.000006	0.510572	-3.34	2.25	IDTIMS	UQ
160183	1465	3.1	14.1	0.130000	0.511803	0.000014	0.510551	-3.75	2.28	MC-ICPMS	SU
160187	1465	4.1	19.9	0.124000	0.511706	0.000007	0.510512	-4.52	2.34	MC-ICPMS	SU
160189	**1449**	5.1	23.1	0.137413	0.511939	0.000025	0.510631	-2.60	2.18	MC-ICPMS	CU
160190	1465	3.2	14.4	0.133000	0.511848	0.000011	0.510568	-3.44	2.26	MC-ICPMS	SU
180701	1465	4.1	18.5	0.134000	0.511805	0.000019	0.510515	-4.47	2.34	MC-ICPMS	SU
180712	**1465**	2.8	13.2	0.128000	0.511838	0.000009	0.510606	-2.69	2.20	MC-ICPMS	SU
180714	**1465**	3.3	15.1	0.131000	0.511809	0.000011	0.510548	-3.82	2.29	MC-ICPMS	SU
Waldburg Dolerite sills											
143446	**1505**	3.5	12.8	0.168416	0.512385	0.000007	0.510719	0.54	1.99	MC-ICPMS	CU
143445	**1505**	2.2	7.9	0.168046	0.512440	0.000005	0.510778	1.69	1.91	IDTIMS	UR
143445	**1505**	2.8	9.9	0.168889	0.512392	0.000006	0.510721	0.59	1.99	IDTIMS	UQ
180717	**1513**	2.6	9.5	0.166029	0.512412	0.000006	0.510761	1.56	1.92	IDTIMS	UR
180717	**1513**	2.3	8.2	0.172324	0.512430	0.000007	0.510716	0.69	1.99	IDTIMS	UQ
207259	**1513**	2.8	10.1	0.166281	0.512437	0.000006	0.510783	2.00	1.89	IDTIMS	UR
206917	**1513**	3.2	12.0	0.163955	0.512376	0.000005	0.510745	1.26	1.95	IDTIMS	UR
Minga Dolerite dykes											
169820	1450	7.6	31.5	0.149551	0.512208	0.000005	0.510783	0.40	1.96	MC-ICPMS	JdLC
169821	1450	5.7	22.0	0.159150	0.512232	0.000008	0.510716	-0.91	2.06	MC-ICPMS	JdLC
169822	1450	5.3	20.6	0.158252	0.512185	0.000005	0.510677	-1.67	2.11	MC-ICPMS	JdLC
169852	1450	5.6	21.8	0.158196	0.512229	0.000008	0.510721	-0.81	2.05	MC-ICPMS	JdLC
169853	1450	6.3	25.9	0.149237	0.512163	0.000004	0.510741	-0.41	2.02	MC-ICPMS	JdLC

NOTES: T_{DM}^2, two-stage depleted mantle model age; 2σ, two sigma; (i), initial

Model age parameters $(^{147}Sm/^{144}Nd)_{DM} = 0.2136$, $(^{143}Nd/^{144}Nd)_{DM} = 0.513163$, $(^{147}Sm/^{144}Nd)_{CHUR} = 0.1960$, $(^{143}Nd/^{144}Nd)_{CHUR} = 0.512630$, $(^{147}Sm/^{144}Nd)_{crust} = 0.11$; Decay constant of $^{147}Sm = 6.54 \times 10^{-12}$

Lab. abbreviations: JdLC, John de Laeter Centre, Curtin University; UQ, University of Queensland; SU, Shimane University (Morris and Pirajno, 2005, 2009)

Other abbreviations: IDTIMS, isotope dilution thermal ionization mass spectrometry; MC-ICPMS, multicollector laser-ablation inductively coupled plasma mass spectrometry

Ages in bold are dated samples; other ages are inferred; the c. 1450 Ma age for the Minga Dolerite dykes is assumed

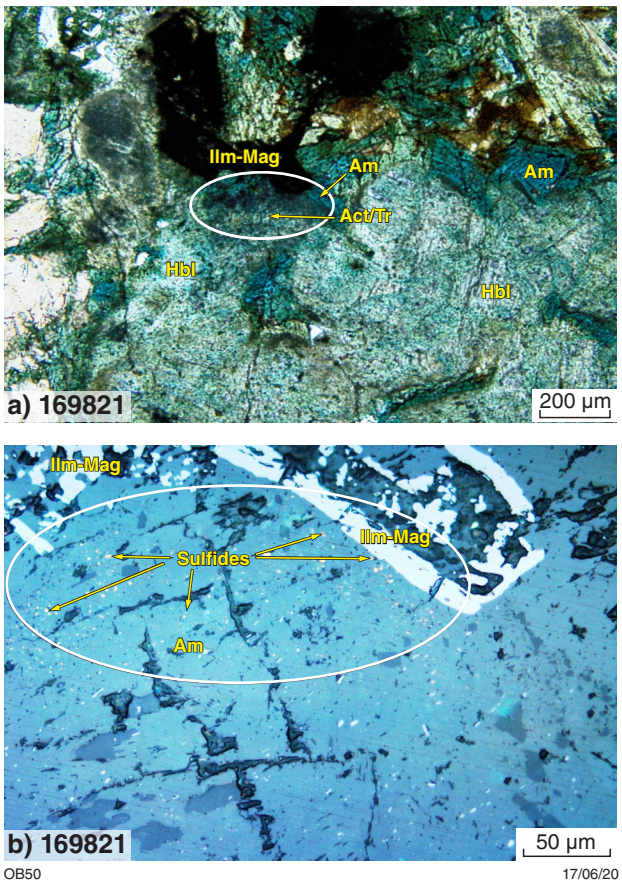

Figure 7. **Photomicrographs of Minga Dolerite dyke sample GSWA 169821, showing: a) hornblende (Hbl) intergrown with ilmenite–magnetite (Ilm-Mag) and rimmed by aqua-blue amphibole (Am) and actinolite-tremolite (Act/Tr), in cross-polarized light; b) higher magnification of the area circled in a), showing very fine-grained sulfide minerals, mainly chalcopyrite, disseminated in actinolite-tremolite and aqua-blue amphibole, in reflected light**

Alteration

Minga dykes show extensive low- to medium-grade metamorphic alteration, which may have affected the mobility of major and trace elements. Values for LOI can be a useful indicator of the degree of alteration (Winchester and Floyd, 1976; Hynes, 1980; Gélinas et al., 1982; Ludden et al., 1982; Morris and Pirajno, 2005), and for the Minga dykes, LOI values are relatively low (<1.13 wt%, Appendix 1). Because both Ti and Zr are typically thought to be relatively immobile during postmagmatic processes, their co-variation with other trace elements can be a useful indicator of element mobility (Cann, 1970; Pearce, 1975; Rollinson, 1993; Pearce, 1996; Blundy and Wood, 2003). As expected, Ti is strongly positively correlated with Zr for the Minga dykes. Positive correlations are also evident between other high field strength elements (HFSE) and rare earth elements (REE) with Zr (Fig. 9), suggesting these trace elements also remained immobile during alteration. There is also no correlation between Ti/Zr and LOI, although variation in Ti/Zr is strongly positively correlated with Mg# and can be attributed to fractional crystallization alone (Appendix 4b). The large ion lithophile elements (LILE), such as K (as K_2O) Cs and Rb, all show clear positive correlations with Zr, whereas Sr varies within a very narrow range and Ba shows considerable dispersion (Appendix 3). None of the LILE elements is clearly correlated with LOI (Fig. 9, Appendix 3). These relationships suggest that primary concentrations of the LILE elements, with the exception of Ba, were also not significantly modified by postmagmatic processes.

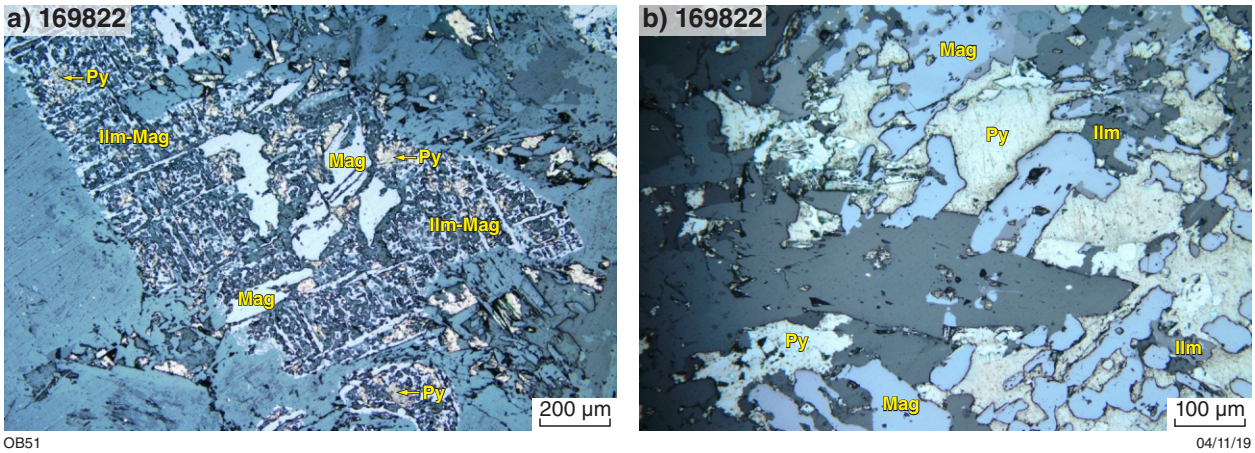

Figure 8. **Photomicrographs (reflected light) of Minga Dolerite dyke sample GSWA 169822, showing: a) subhedral ilmenite–magnetite (Ilm–Mag) crystals with exsolution texture, overgrown by pyrite (Py); b) pyrite penetrating and/or surrounding ilmenite–magnetite crystals**

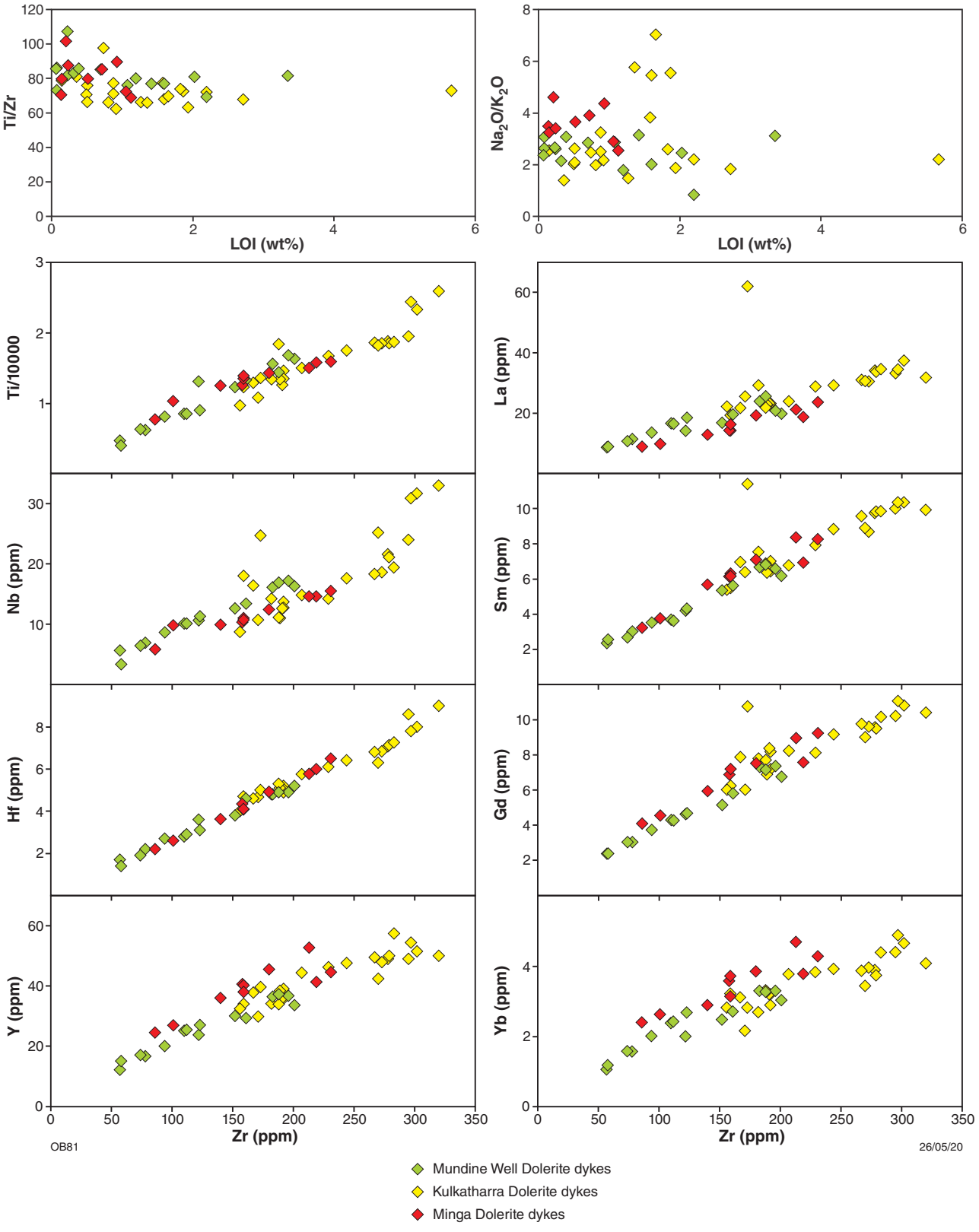

Figure 9. Variations in major and trace elements with LOI and Zr concentration, for Minga, Kulkatharra, and Mundine Well Dolerite dykes

Major and trace element variations

The Minga dykes are tholeiitic rocks (Fig. 10). Compared with normal mid-oceanic basalt (N-MORB), they have relatively evolved compositions, with high K_2O (0.63%) and P_2O_5 (0.24%) (c.f. N-MORB values of 0.07 and 0.11 respectively; Sun and McDonough, 1989) and low average MgO (5.4%), Mg# (40) and Ni (57 ppm) (Table 1, Appendix 1). They are enriched in all incompatible trace elements (REE, HFSE, LILE, Th, U), with weakly to moderately fractionated (i.e. negatively sloping) mantle-normalized trace element patterns ($(La/Yb)_N$ = 2.7 – 4.0) and small to moderate negative Nb anomalies (Table 1, Appendix 1, Fig. 11). Such patterns reflect a bulk source that was more enriched in compatible trace elements than primitive mantle and that included a low-Nb/La, high-Th/Nb 'crustal' component (Fig. 15, Appendix 1). Because the moderately weak negative Nb anomalies (Nb/La up to 0.8) limit the amount of crustal material present within the bulk source for these rocks, it is possible that the primitive parental magmas approximated enhanced mid-ocean ridge basalt (E-MORB) in composition.

Major element oxides, Cr, and Ni vs Mg# exhibit distinct correlations (Fig. 12). Positive correlation of Ni, Cr, and CaO with Mg#, is consistent with fractional crystallization of a mafic silicate phase. The generally evolved nature of the Minga Dolerite magmas (e.g. Mg# = 32–49) reflects compositions far removed from primary mantle magmas. This is consistent with the narrow range of low Ni concentrations (39–78 ppm) and with petrographic observations confirming an absence of olivine, and suggests significant olivine fractionation did not occur within the sampled compositional range. Scattered positive correlations of Sc/V with Mg# and decreasing Sr/Nd with increasing Zr, suggest fractionation controlled by removal of clinopyroxene and plagioclase, respectively (Fig. 12). This is consistent with the plagioclase- and augite-dominated mineralogy, although the lack of significant negative Eu anomalies in mantle-normalized trace element diagrams (Fig. 11) also suggests the amount of plagioclase fractionation was not large.

The PGE and Au analyses of selected dolerite samples (Appendix 1) indicate relative enrichment in Au (8.2 – 10.5 ppb), Pd (1.1 – 24.1 ppb), and Pt (5.6 – 6.8 ppb), but very low concentrations of other PGE elements. The Pt, Pd, and Au budgets may have been controlled by the abundance of finely disseminated sulfide minerals, particularly chalcopyrite and bornite (Haluzova et al., 2015), although Au and Pt- and Pd-bearing minerals, and associated mineral assemblages were not investigated in this study.

The Th/Nb ratio of mafic rocks can be used to assess the role of crustal contamination (Pearce and Peate, 1995; Pearce, 2008). In a Th/Yb vs Nb/Yb diagram (Fig. 13), Minga dyke samples plot above the MORB-OIB array, indicating a bulk source that included a crustal component. Together, the data appear to form an indistinct trend to higher Th/Yb at relatively constant Nb/Yb ratios. Such trends are consistent with progressive contamination of mantle-derived magmas with Th-rich crustal material.

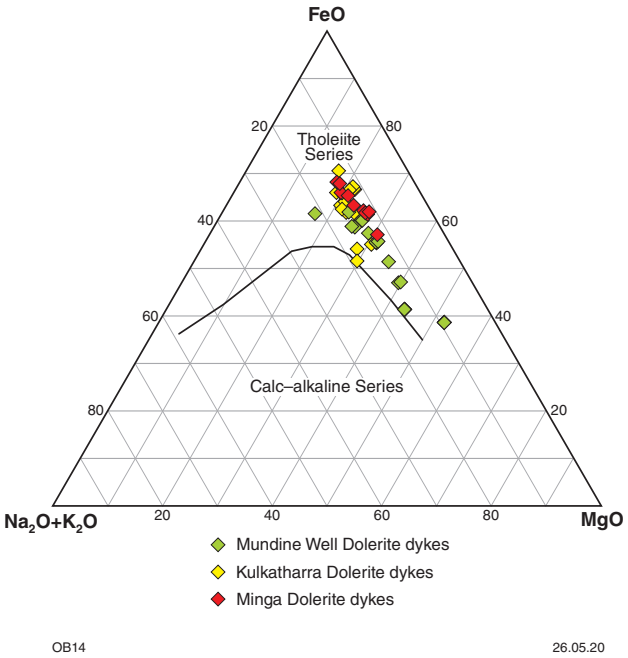

Figure 10. Ternary AFM (alkalis–iron–magnesium) classification diagram (Irvine and Baragar, 1971) showing tholeiitic character of the Capricorn Orogen dolerite dykes

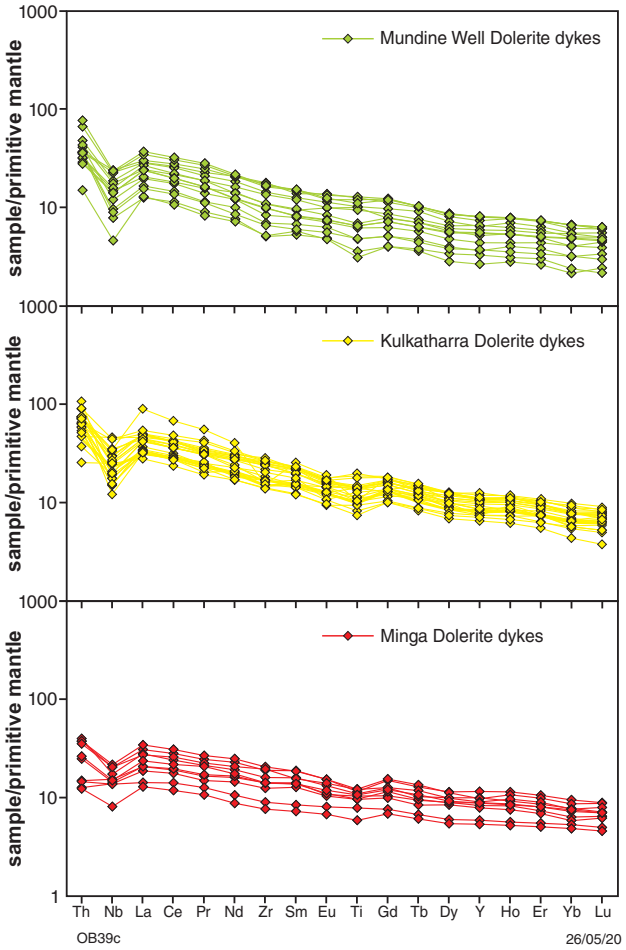

Figure 11. Trace element diagrams for Minga, Kulkatharra, and Mundine Well Dolerite dyke samples. Results are normalized to primitive mantle (Sun and McDonough, 1989)

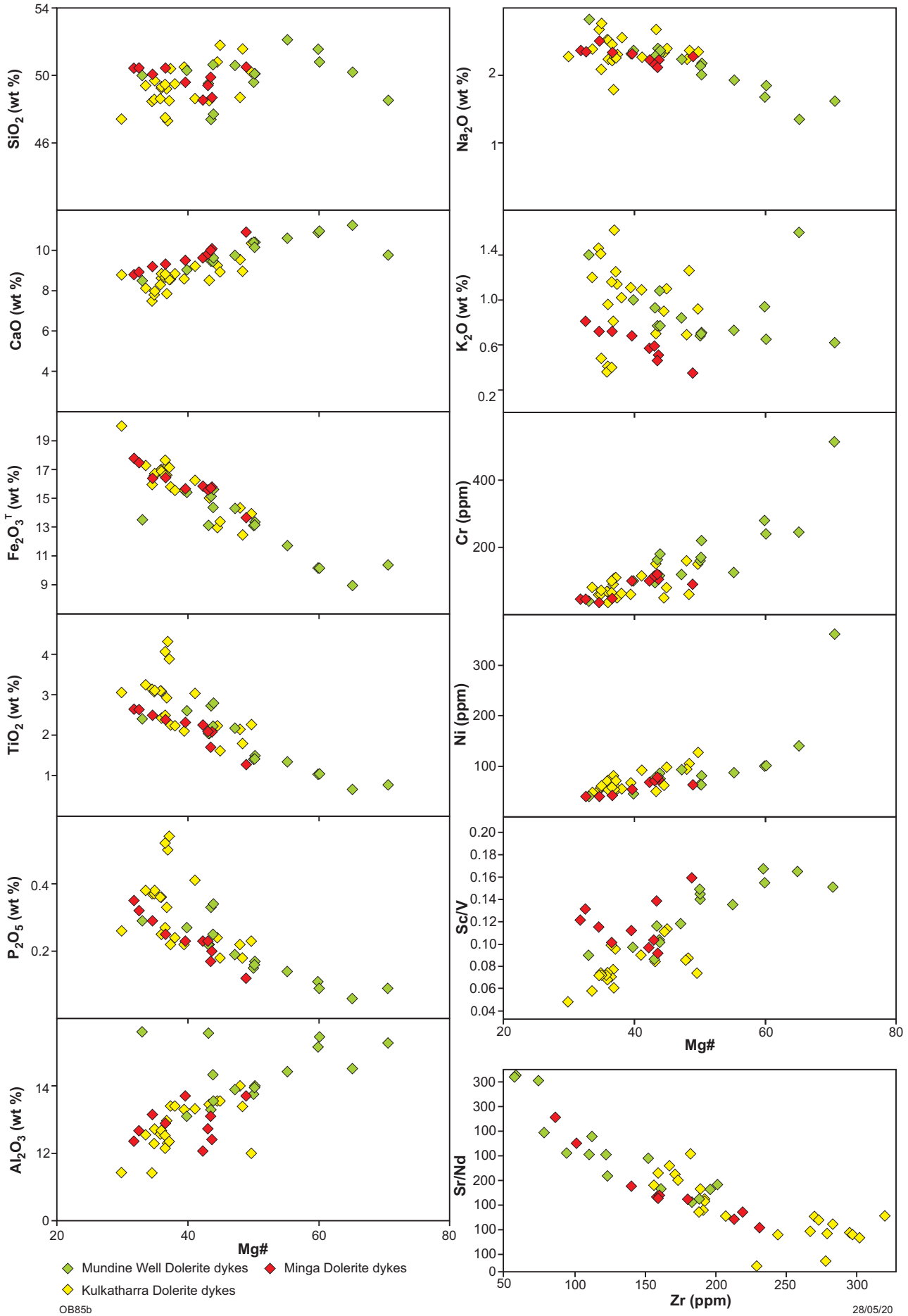

Figure 12. Binary variation diagrams for Minga, Kulkatharra, and Mundine Well Dolerite dyke samples, showing representative correlations of major element oxides

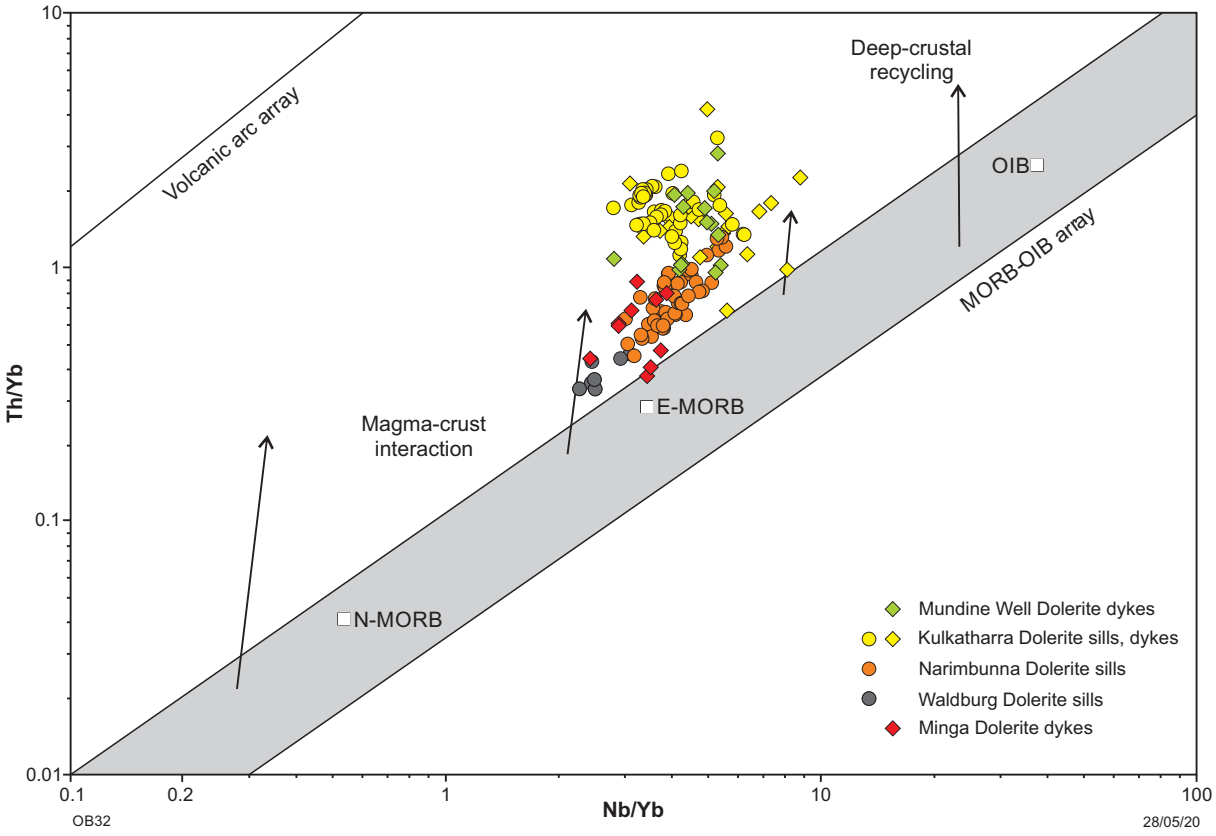

Figure 13. Th/Yb vs Nb/Yb discrimination diagram (Pearce, 2008) for dykes and sills of the Minga, Kulkatharra, Mundine Well Dolerites, Waldburg, and Narimbunna Dolerites. Although the trends for the Minga dykes are not definitive, they are probably most consistent with these dykes representing mantle-derived magmas, possibly with compositions resembling E-MORB, that were more or less continuously contaminated through assimilation of crustal material during emplacement. The Mundine Well Dolerites and a group of Kulkatharra Dolerites probably formed in a similar way to the Minga dykes based on trends displayed in this diagram. The trends for Narimbunna Dolerite sills and many of the Kulkatharra Dolerites are more consistent with formation through remelting of a previously subduction-modified mantle source, followed by more or less closed-system compositional evolution during emplacement. Abbreviations: E-MORB, enriched mid-oceanic ridge basalt; N-MORB, normal mid-oceanic ridge basalt; OIB, oceanic island basalt

Sm–Nd isotopes and potential magma sources

Samples of Minga dykes yield a relatively narrow range of initial $^{143}Nd/^{144}Nd_{(i)}$ ratios, from 0.510677 to 0.510783, and $\varepsilon_{Nd(i)}$ from –1.67 to 0.40 (Table 2), corresponding to depleted mantle model ages (T_{DM}^{2}) between 2.11 and 1.96 Ga (Fig. 14). Minga dykes were most likely derived from a source with a Nd isotope signature somewhere between depleted mantle (DM) and CHUR, although the precise composition cannot be determined. The present, relatively non-radiogenic compositions, combined with weak but persistent negative Nb anomalies (Nb/La typically <0.8) (Figs 11, 15) clearly suggest a bulk source that included an evolved 'crustal' component. Minimal, but systematic, variations in geochemical proxies for crustal contamination (e.g. Morris and Pirajno, 2005; Wang, 2013; Wang et al., 2014), such as weak correlations between Th/La and Mg# (Fig. 15), might suggest that this crustal component was progressively added to the evolving magma through a continuous process of crustal assimilation, but variations between $\varepsilon_{Nd(i)}$ and SiO_2, Th/La, Nb/La, La/Sm, or Mg# (Fig. 16), imply the suite becomes geochemically less evolved (rather than more evolved) (i.e. less siliceous, higher Mg#, lower La/Sm) with an increasing crustal contribution. If the crustal component in these rocks was added via a continuous process of crustal assimilation, the assimilated crust was old (Nd isotope constraint) and primitive mafic crust with an unusually high Th concentration. Old mafic forearc crust might be a candidate for such an unlikely crustal component.

Comparison with Narimbunna Dolerite sills

Sills of Narimbunna Dolerite and Minga dykes are highly altered, and are similar in mineralogy, including primary plagioclase and clinopyroxene replaced by low- to medium-grade metamorphic minerals, typically amphibole, chlorite, hornblende, and epidote. Minga dykes are more extensively altered than sills, and typically exhibit complete replacement of primary minerals, particularly pyroxenes, by compositionally variable amphiboles and associated sulfide minerals (e.g. pyrite, chalcopyrite and bornite). Clouded plagioclase is observed only in Minga dykes (Fig. 6a), implying that the dyke exposures originated at significantly greater depth than those of Narimbunna sills (e.g. Halls and Zhang, 1995, 1998).

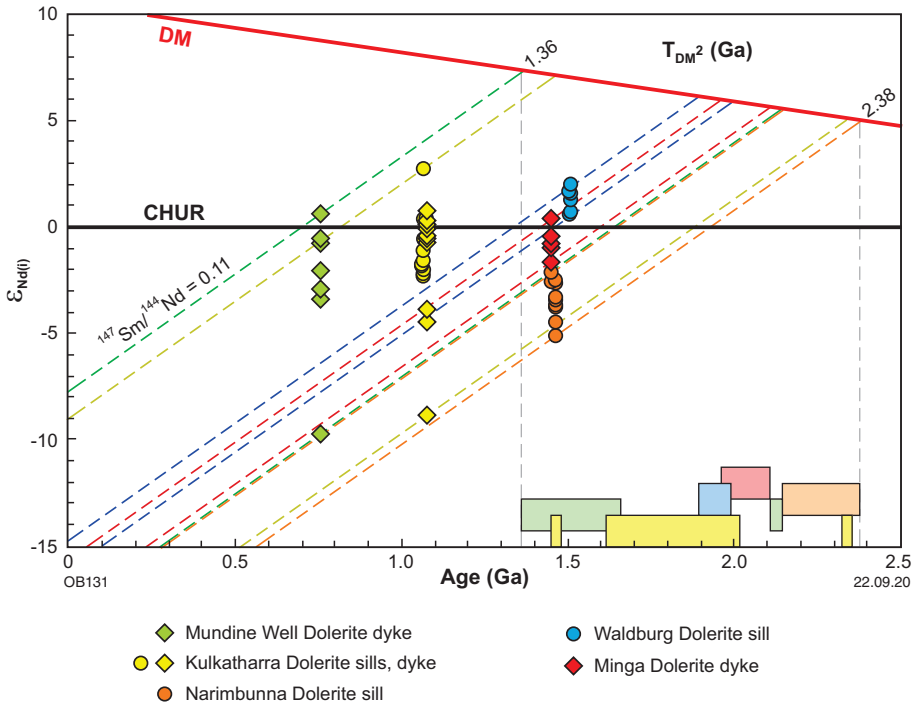

Figure 14. Sm–Nd evolution diagram for dykes and sills of the Minga, Waldburg, Narimbunna, Kulkatharra, and Mundine Well Dolerites. The range of two-stage DM model ages (T_{DM}^{2}) is indicated by coloured boxes for each suite, values for the undated Minga Dolerite dykes are based on an assumed age of c. 1450 Ma. Abbreviations: DM, depleted mantle; CHUR, chondritic uniform reservoir. Sm–Nd isotope data are compiled for dykes and sills in Table 2

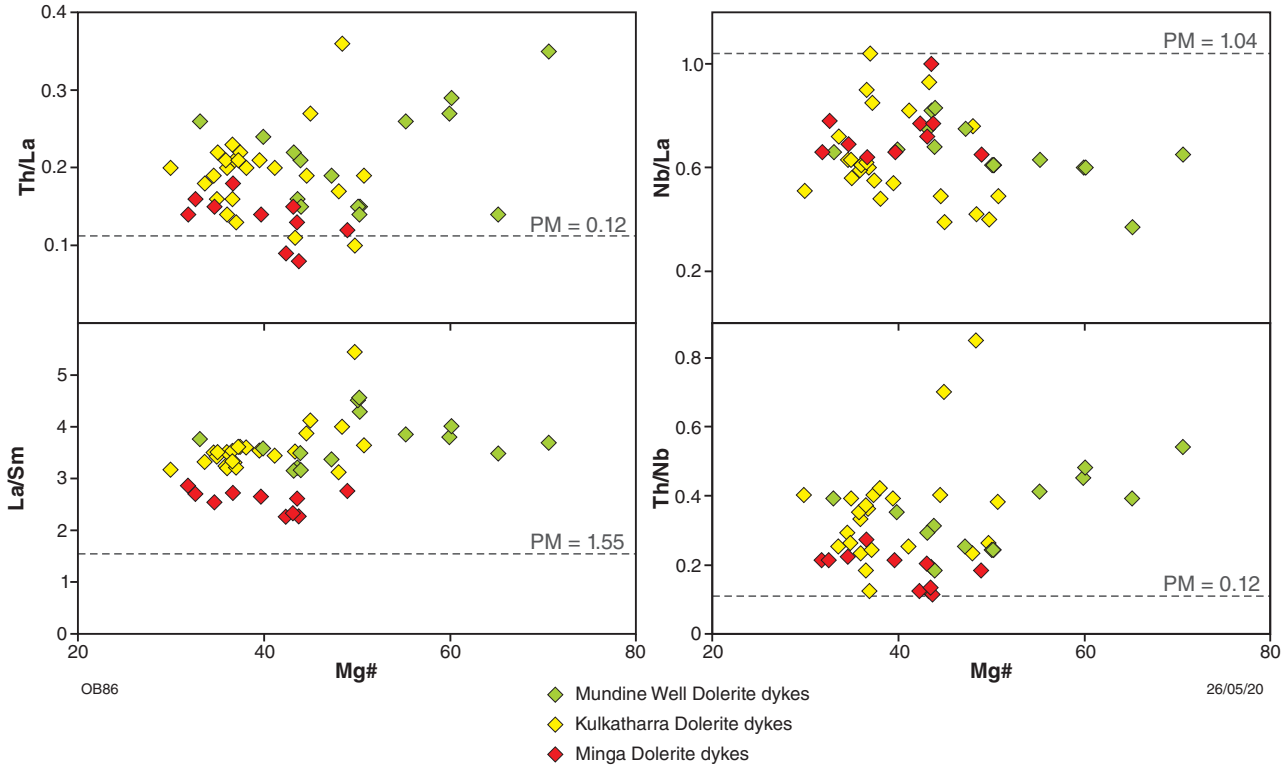

Figure 15. Binary variation diagrams for Narimbunna, Kulkatharra, and Mundine Well Dolerite dyke samples, showing geochemical characteristics of each group in terms of REE–HFSE ratios relative to primitive mantle (PM). Abbreviations: Mg#, molecular Mg/(Mg + total Fe)

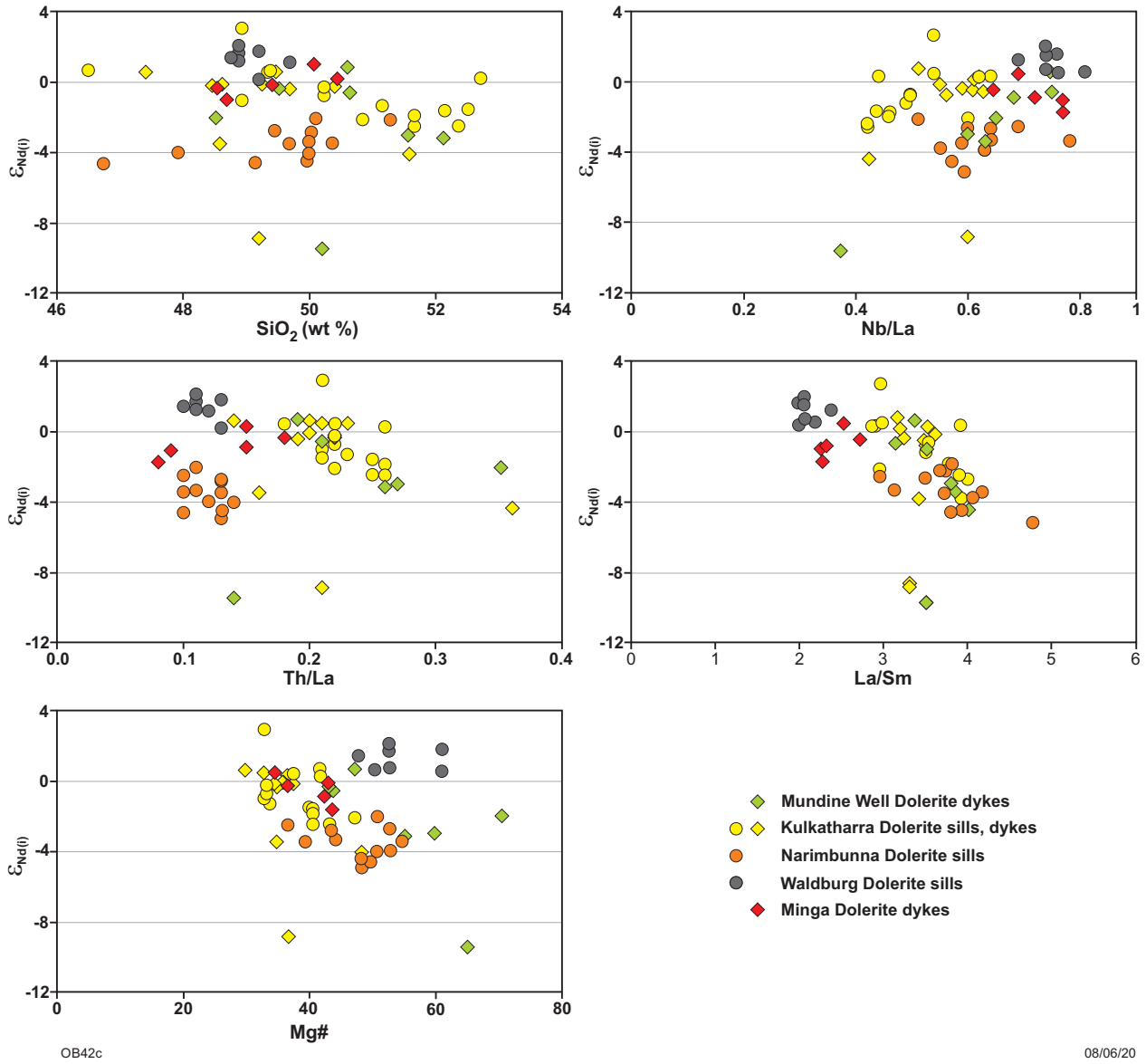

Figure 16. Variation of $\varepsilon_{Nd(i)}$ with SiO_2, Nb/La, Th/La, La/Sm, and Mg# for Minga, Kulkatharra, Mundine Well, Waldburg, and Narimbunna Dolerite samples, examining characteristic correlations as geochemical proxies for crustal contamination. $\varepsilon_{Nd(i)}$ is calculated using initial $^{143}Nd/^{144}Nd$ values corrected to crystallization age

A main objective of this study was to assess whether the Narimbunna Dolerite and Minga dykes are petrogenetically related. Comparing trace element ratios for the two groups, there are subtle, but persistent, differences, with the Minga dykes typically having (for example) lower La/Sm, and Nb/Y ratios (Appendix 6a). In particular, bivariate plots of La and Th against Zr (Fig. 17), emphasize the distinctions between the Narimbunna Dolerite and Minga dykes, each group having distinct linear trends (Minga dykes with lower La/Zr and Th/Zr ratios) that extrapolate to the origin and thus, in principle, define the element ratio of the bulk source. These contrasting trends make a direct genetic relationship between the Narimbunna Dolerite and Minga dykes highly unlikely. The constant trends in La/Zr, Th/Zr and La/Sm (Fig. 17), in the case of the Minga dykes, are surprising given the evidence (above) indicating a continuously changing bulk source composition reflecting continuous crustal contamination of old mafic crust, and perhaps suggests that the alternative origin through extraction from an already subduction-modified mantle source, is more likely. There are presently too few data to indicate which of the two petrogenetic alternatives is most likely.

In a Th/Yb vs Nb/Yb diagram (Fig. 13), Narimbunna Dolerite samples plot above, and trend parallel to, the MORB-OIB array, suggesting that these magmas were derived from a source that already possessed a relatively homogeneous and high-Th/Nb ratio, probably weakly subduction-modified subcontinental lithospheric mantle. However, the Narimbunna Dolerite has distinctly less radiogenic Nd isotope compositions than the Minga dykes (Fig. 16). Combined, these observations strongly suggest that there is no petrogenetic relationship between Narimbunna Dolerite and Minga dykes.

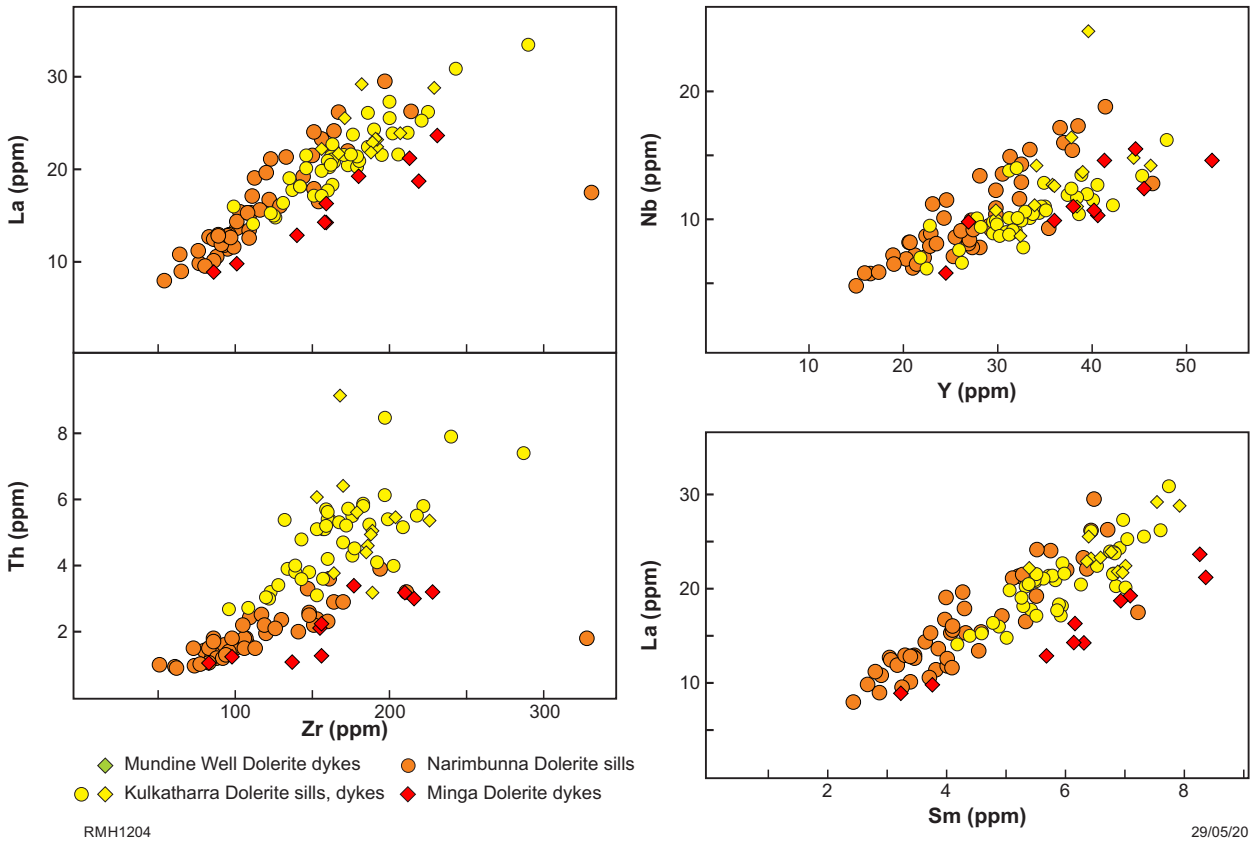

Figure 17. Variation of selected incompatible trace elements in Minga, Narimbunna, Kulkatharra, and Mundine Well Dolerite samples

Summary

In the western Capricorn Orogen, sills of Narimbunna Dolerite and dykes of the Minga Dolerite are geochemically and petrogenetically distinct, although they were initially presumed to be petrogenetically related based on cursory geochemical similarities and on similar primary and alteration mineralogy. In both the sills and dykes, primary plagioclase and pyroxene are extensively replaced by low- to medium-grade metamorphic minerals, such as amphiboles, clinozoisite–epidote, biotite, and sericite. Titanite, apatite, pyrite, and chalcopyrite are common accessory minerals. Both dykes and sills are tholeiites, characterized by enriched REE and HFSE profiles. Although trace element profiles for the dykes and sills are broadly similar, there are several subtle distinctions in trace element ratios, and in particular, in trends in plots of La and Nb vs Zr, and in Th/Yb vs Nb/Yb. Together with distinctive Nd isotope compositions, the data suggest that the dykes and sills almost certainly formed independently from each other from compositionally distinctive source rocks through contrasting petrogenetic processes. The Narimbunna Dolerite sills formed through remelting of a previously subduction-modified mantle source (i.e. already contaminated) with an elevated Th/Nb ratio, and underwent essentially closed-system compositional evolution during emplacement. It is not clear if the Minga dykes formed through a similar process or if they represent mantle-derived magmas, possibly with compositions resembling E-MORB, that were more or less continuously contaminated through assimilation of crustal material during emplacement. Because the Minga dykes cannot be correlated with the c. 1.5 Ga Narimbunna sills, the age of the dykes remains unknown, and the Nd isotope characteristics of both the mantle source and the crustal component remain obscure.

Kulkatharra Dolerite dykes

Field observations

Dykes and sills of the c. 1075 Ma Kulkatharra Dolerite occur throughout the central Capricorn Orogen, where they mainly intrude low-grade sedimentary rocks of the Edmund and Collier Basins (Thorne, 2016a,b; Blay et al., 2018c). Kulkatharra dykes also intrude low-grade metasedimentary and metavolcanic rocks of the southern 2008–1799 Ma Ashburton Basin (Thorne, 2018a) and the 1799–1738 Ma Blair Basin (Thorne, 2018b) on Ullawarra, Capricorn and Kenneth Range (Fig. 2). They intrude sedimentary rocks of the Bresnahan, Capricorn, and Wyloo Groups (Thorne, 2015, 2020; Thorne and Johnson, 2018). On Mangaroon and Edmund a few north-northeasterly and northeasterly striking dykes also cut Paleoproterozoic granitic rocks of the Durlacher Supersuite (Sheppard et al., 2018a), and the Pooranoo and Leake Spring Metamorphics (Sheppard and Johnson, 2018, 2019). From field observations and aeromagnetic data (Figs 2, 4), the

majority of the Kulkatharra dykes appear to terminate against the Talga – Mount Vernon Fault System and the Godfrey Fault.

Most Kulkatharra Dolerite dykes trend northwest or northeast, although some are arcuate and some are oriented east–west. Kulkatharra dykes are typically exposed as rubbly outcrops within creek beds and banks, and to a lesser degree, along slopes of low ridges. The dykes are typically extensively fractured and weathered, and spheroidal weathering is common. Contacts with host rocks are generally not exposed, although locally the country rocks are bleached (e.g. AMTBAN002902, 503760E 7412416N) or exhibit epidote alteration near dyke margins (e.g. AMTBAN002901, 503805E 7412021N). On Tangadee, sedimentary rocks adjacent to a 150 m-wide, northwesterly trending, medium- to coarse-grained dolerite dyke display discontinuous small-scale folding (e.g. HNCTGE002843, 682369E 7327461N).

Northwesterly to northeasterly trending dykes are poorly exposed, mainly within creek beds. They have interpreted strike lengths of 3–70 km and are mainly 1–20 m wide (rarely up to 150 m). East-trending dykes are typically well exposed, 1.5 m to 80 m wide (e.g. AMTBAN002907, 538437E 7384023N) and 7–15 km long, although a few have interpreted strike lengths of up to 200 km (Fig. 2). The longer easterly trending dykes change to a more northeasterly trend close to their terminations at the Talga – Mount Vernon and Godfrey Faults.

Three concentric arcuate dykes, spaced about 15–30 km apart, occur on Capricorn and western parts of Ashburton and Kenneth Range (Fig. 2). The inner arcuate dyke has an interpreted strike length of about 17 km, whereas the outermost dyke is approximately 52 km long. Both arcuate dykes display high-intensity positive aeromagnetic anomalies (Figs 3, 4), although their measured thicknesses are <5 m, and appear to focus on a relatively small (~4 km in diameter), semicircular, high-intensity aeromagnetic anomaly (Fig. 3) that closely coincides with a Kulkatharra? Dolerite sill within Edmund Group sedimentary rocks on Ullawarra (e.g. OXBBAN000181, 446497E 7412958N).

Petrography

Kulkatharra Dolerite dykes comprise two distinct petrographic types, summarized here and described in detail in Appendix 2. Type 1 dolerite occurs mainly in arcuate, and to a lesser degree, in northwesterly and easterly trending dykes on Capricorn, Kenneth Range, and Ashburton (Fig. 2). Typically, Type 1 dykes are mainly fine grained and moderately altered. They are generally porphyritic to glomeroporphyritic with a groundmass that exhibits intersertal to intergranular, or less commonly, hyalopilitic textures or are recrystallized to a brownish cryptocrystalline matrix (Appendix 2 Fig. 2.13a,b). Type 1 dykes contain variable amounts of cumulophyritic clusters of primary plagioclase–augite–alkali-feldspar–opaque minerals with accessory biotite, pyrite and lesser apatite, and contain mainly plagioclase and pyroxene phenocrysts. Two generations of plagioclase and pyroxene are highlighted: 1) primary crystals, large in size, typically long prismatic and/or elongated; 2) secondary crystals, small acicular and/or short prismatic plagioclase; granular anhedral and/or short prismatic pyroxene (Appendix 2 Figs 2.13a,b, 2.17a,c). Type 1 dykes also contain up to 30% titanomagnetite and/or ilmenite in both groundmass and phenocrysts, making them slightly magnetic.

Type 2 dolerite occurs mainly in northeasterly and easterly trending dykes on Ullawarra, Elliot Creek, and southern Capricorn (Fig. 2). These rocks are mainly fine to medium grained, exhibit subophitic textures, and may include rare porphyritic or glomeroporphyritic patches. Type 2 dykes contain subequal primary plagioclase and augite, lesser granophyre, titanomagnetite, ilmenite, and minor hematite, biotite, alkali feldspar, and quartz (Appendix 2 Fig. 2.18). Accessory minerals typically include sulfides (mainly chalcopyrite and pyrite), and traces of baddeleyite, zircon, and zirconolite. Type two dykes locally exhibit abundant epidote alteration.

Both dolerite types contain abundant skeletal and dendritic titanomagnetite and/or ilmenite crystals and are also enriched in very fine-grained opaque minerals surrounded by haloes of radiation damage (Appendix 2 Figs 2.14, 2.16). The presence of skeletal and dendritic iron–titanium oxide minerals, two generations of plagioclase and pyroxene phenocrysts, together with microfracturing and dislocation of phenocrysts (Appendix 2), probably indicates initial slow cooling followed by abrupt, rapid cooling conditions during dyke intrusion (Rice et al., 1971; Kretz, 2003). In addition, the presence of hyalopilitic textures is consistent with near-surface emplacement (Nockolds et al., 1978), and amygdaloidal textures indicate both near-surface emplacement and volatile-rich magma. Porphyritic and glomeroporphyritic textures also suggest a complex cooling and crystallization history (Nockolds et al., 1978).

Geochronology

Crystallization ages for five Kulkatharra Dolerite sills (Blay et al., 2018c) range from c. 1083 to 1067 Ma, with samples of four sills yielding a mean age of 1075 ± 3 Ma; two samples of one sill yielded a significantly older age of 1083 ± 4 Ma and may represent a separate episode of dolerite intrusion. Geochronology data are available for zircons from samples of two Kulkatharra Dolerite dykes and a siltstone within the baked contact of a large Kulkatharra dyke. Although several dykes sampled for geochronology are enriched in Zr (156–320 ppm, Appendix 1), most did not yield primary zircon, baddeleyite, or zirconolite for geochronology, suggesting that Zr resides in minerals such as titanite, ilmenite, clinopyroxene, amphibole, magnetite, or orthopyroxene (Bea et al., 2006).

Sample GSWA 169827 was obtained from an easterly trending, medium- to coarse-grained quartz dolerite dyke (e.g. 468325E 7404079N) intruded into sandstone and siltstone of the Gooragoora Formation of the lower Edmund Group (Thorne et al., 2004, 2018c). Two SHRIMP U–Pb analyses of a single zircon in polished thin section yielded a weighted mean $^{207}Pb^*/^{206}Pb^*$ date of 1081 ± 27 Ma, interpreted as the crystallization age (B Rasmussen, written comm., 2013).

Sample GSWA 143497 was obtained from a 20 cm-wide, fine-grained dolerite dyke (HNCTGE000746, 682232E

7327811N) intruded into a Kulkatharra Dolerite sill, itself emplaced within sandstone of the 1590–1455 Ma Ullawarra Formation of the Edmund Group (Thorne, 2018d). The sampled dyke is about 100 m northeast of, and parallel to, a 150 m-wide, northwesterly trending Kulkatharra Dolerite dyke that offsets the Kulkatharra Dolerite sill and adjacent units (Thorne and Cutten, 2010). Twenty-one analyses of 20 zircons from the 20 cm-wide dolerite dyke yielded dates of 2988–1707 Ma, interpreted as the ages of inherited zircons (Lu et al., 2017), and do not constrain the age of the dyke.

About 450 m to the south-southeast (e.g. HNCTGE000912, 682427E 7327399N), a sample of siltstone of the Ullawarra Formation was collected within the baked contact of the 150 m-wide, northwesterly trending Kulkatharra Dolerite dyke described above – less than 1 m from the contact. Detrital zircons in the sample yielded ages of 3240–1785 Ma (GSWA 189219, Wingate et al., 2014). However, two analyses of one zircon yielded a concordia age of 1069 ± 19 Ma, which is too young to represent the age of a detrital zircon in the Edmund Group. Assuming that the siltstone is not younger than expected, the young dates for the zircon might be explained by complete isotopic resetting of the zircon (i.e. loss of all radiogenic Pb) in the contact aureole of the dyke during intrusion, in which case the date of 1069 ± 19 Ma could be interpreted as the age of the dyke. Zircons formed in contact rocks melted by intrusion of an Ordovician mafic dyke in southern Siberia have been described and dated by SHRIMP U–Pb methods (Gladkochub et al., 2013).

Geochemistry

Alteration

Kulkatharra Dolerite dykes are significantly less altered and metamorphosed than those of Narimbunna Dolerite and Minga dykes. Most show only low degrees of postmagmatic alteration, although there are local exceptions. LOI is up to 5.7%, but typically is relatively low, averaging 1.4% (Appendix 1). Strong positive correlations in HFSE and REE with Zr (Fig. 9), suggest that primary concentrations of these trace elements have not been significantly modified by alteration. The LILE show poor correlations with Zr (Appendix 3) and together with high dispersion of Na_2O/K_2O ratios over a range of LOI (Fig. 9), may imply that LILE concentrations have been modified by alteration processes, although much of this variation might also be linked to inhomogeneous distribution of plagioclase glomerocrysts.

Major and trace element composition

Kulkatharra Dolerite dykes have tholeiitic compositions (Fig. 10). They display significant variations in SiO_2 (47.3 – 51.8%), TiO_2 (1.6 – 4.3%), $Fe_2O_3^T$ (12.5 – 20.0%), P_2O_5 (0.18 – 0.54%), CaO (3.7 – 10.4%), and K_2O (0.4 – 1.6%) (Fig. 12, Table 1). Kulkatharra dykes have relatively low concentrations of MgO (4.3 – 7.0%), moderate Na_2O (1.8 – 3.0%), and highly variable Mg# (29.9 – 50.7, average 39.4) (Table 1, Appendix 5). They are also characterized by high and variable V (234–726 ppm), and low and variable Cr (36–160 ppm) and Ni (48–127 ppm) (Table 1, Appendix 5). Their major and trace element concentrations are distinctly different from those of Minga and Mundine Well dykes (Figs 11, 12; Table 1). Average concentrations of TiO_2 and P_2O_5, for example, are higher than in Minga and Mundine Well dykes.

Kulkatharra Dolerite dykes are markedly enriched in LREE and HFSE (principally Ti, Nb and Zr) (Table 1, Appendices 1, 5). They display a wide range of REE and HFSE concentrations, such as La (19–62 ppm), Ce (42–121 ppm), Gd (6–11 ppm), and Nb (9–33 ppm). On Edmund, a northeasterly trending dyke exhibits significantly higher LREE concentrations than other Kulkatharra dykes, e.g. La (62 ppm), Ce (121 ppm), and Pr (15 ppm), together with elevated Ba (1480 ppm), Sr (550 ppm), Nd (55 ppm), and Ni (127 ppm) (GSWA 207231, Appendix 1). This anomalous dyke will not be considered further here. Bivariate plots of incompatible trace elements (Fig. 15) typically show more dispersion for the Kulkatharra dykes than for the Minga dykes, although primitive mantle-normalized trace element patterns for the Kulkatharra dykes are essentially parallel which each other (Fig. 11). The normalized patterns indicate moderate to strong fractionation in both light REE [$(La/Sm)_N$ = 2.0 – 3.5, average 2.3) and heavy REE ($(Gd/Yb)_N$ = 1.6 – 3.2, average 2.0], and an average Eu/Eu* of 0.87 (Appendix 1). This is accompanied by highly variable, on average moderately elevated, Th/La (0.10 – 0.36), Th/Nb (0.12 – 0.85), and La/Sm (3.1 – 5.4), and relatively low Nb/La (0.4 – 1.0) compared to primitive mantle (Sun and McDonough, 1989) (Fig. 15, Appendix 1).

As a group, the Kulkatharra Dolerite dykes show positive correlations for Al_2O_3, CaO, Cr, and Ni vs Mg#, whereas $Fe_2O_3^T$, TiO_2, and P_2O_5 show negative correlations (Fig. 12). Values for Al_2O_3, TiO_2, P_2O_5, and Cr contents are relatively dispersed within a wide range of Mg# (29.89 – 50.71). Relatively low and variable Cr and Mg# values, and generally low Ni contents (Table 1, Appendices 1, 5), together with weak-to-moderate positive correlations between Cr and Ni with Mg# (Fig. 12) indicate fractional crystallization of phases such as olivine and clinopyroxene (± orthopyroxene) (Pang et al., 2016; Humbert et al., 2018). However, petrographic observations indicate that clinopyroxene rather than olivine was the dominant fractionating phase. Trends to decreasing Sr/Nd with increasing Zr (Fig. 12) indicate limited plagioclase fractionation, and the lack of significant negative Eu anomalies in primitive mantle-normalized trace element diagrams (Fig. 11) also suggests the amount of plagioclase fractionation was not large.

The additional dispersion in trace element ratios shown by the Kulkatharra Dolerite dykes (Fig. 17, Appendix 4) might reflect very small variations in bulk source compositions, and some of these variations appear to be geographically constrained. For example, dykes in the northwestern extent of the geographical range of the Kulkatharra Dolerite dykes, mainly west of longitude 117.15º, are generally enriched in TiO_2 and P_2O_5 (Fig. 18) and in incompatible trace elements, with generally higher La/Zr, Yb/Zr, Nb/Zr and Nb/Ti than the low-Ti–P population (Low-Ti) to the southeast (Fig. 19). These dykes to the northwest can be divided into medium- and high-Ti–P groups (Medium-Ti and High-Ti) with minimal geographical overlap in outcrop extent, and each distinct in terms of (for example) Nb/Zr, Nb/Ti, Nb/La, and La/Zr. The Medium-Ti group broadly

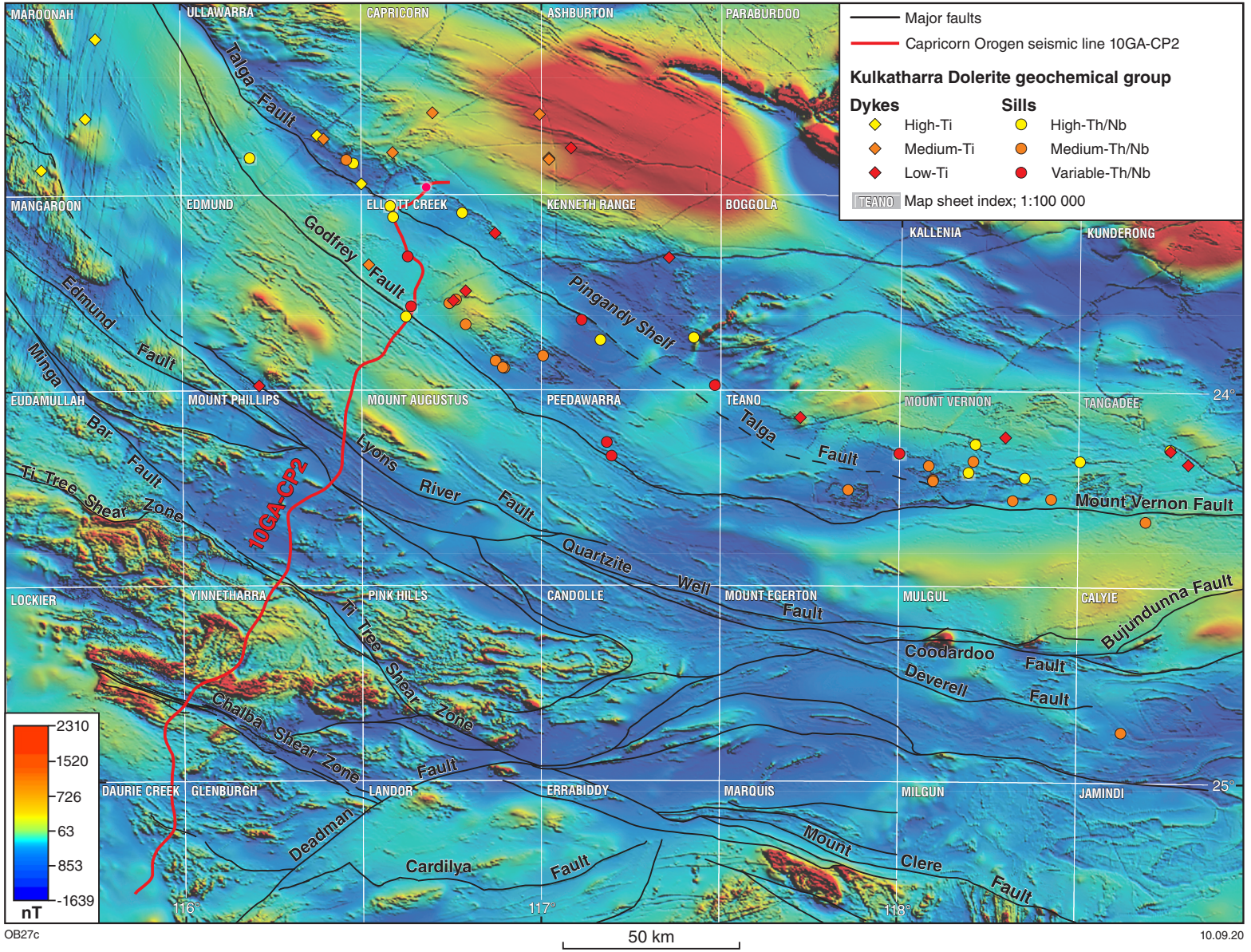

Figure 18. Compositional groups within Kulkatharra Dolerite samples. The base map is total magnetic intensity image (80 m pixel resolution) of the western Capricorn Orogen, showing major faults

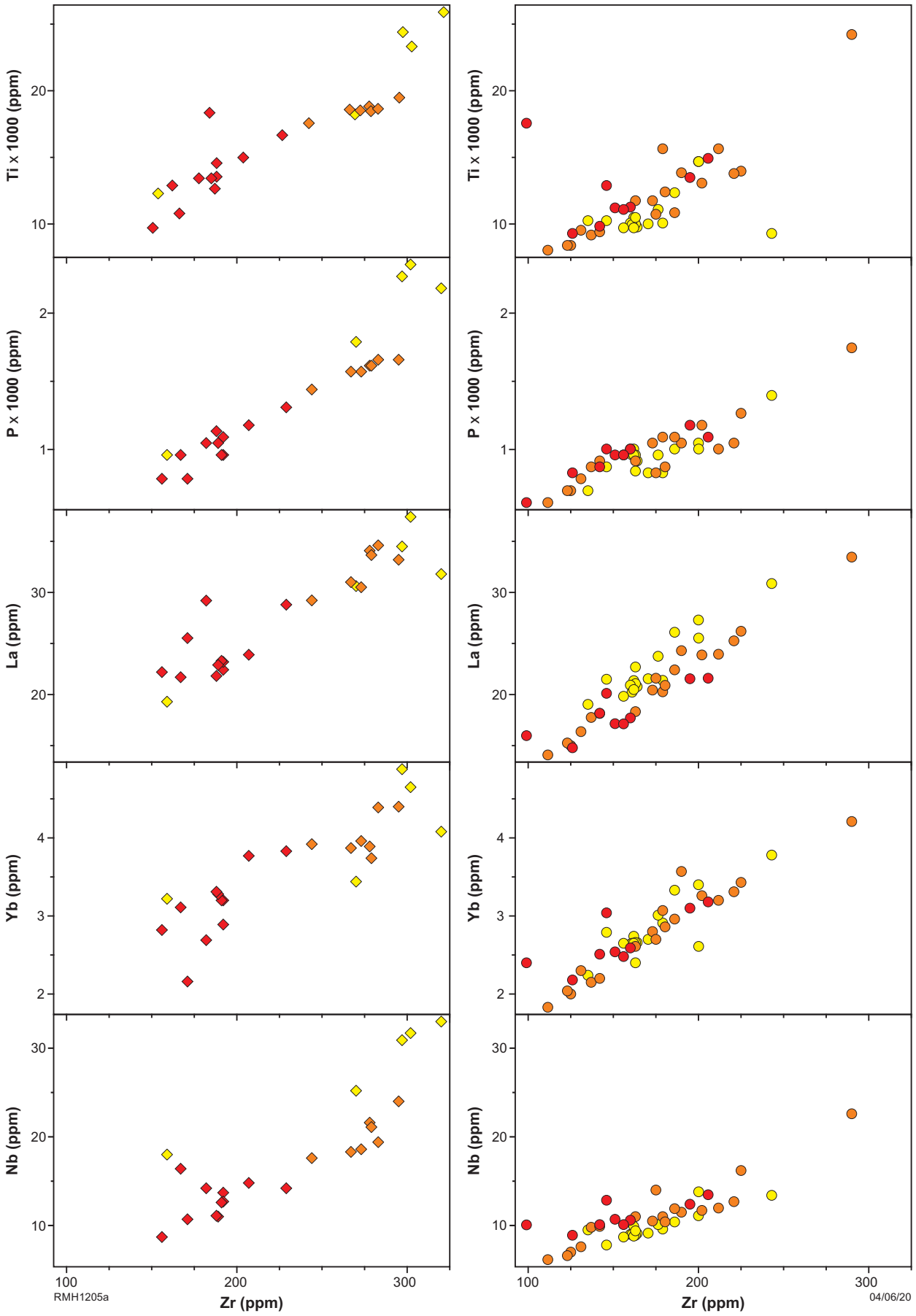

Figure 19. Variation of selected elements vs Zr and Nb within Kulkatharra Dolerite samples

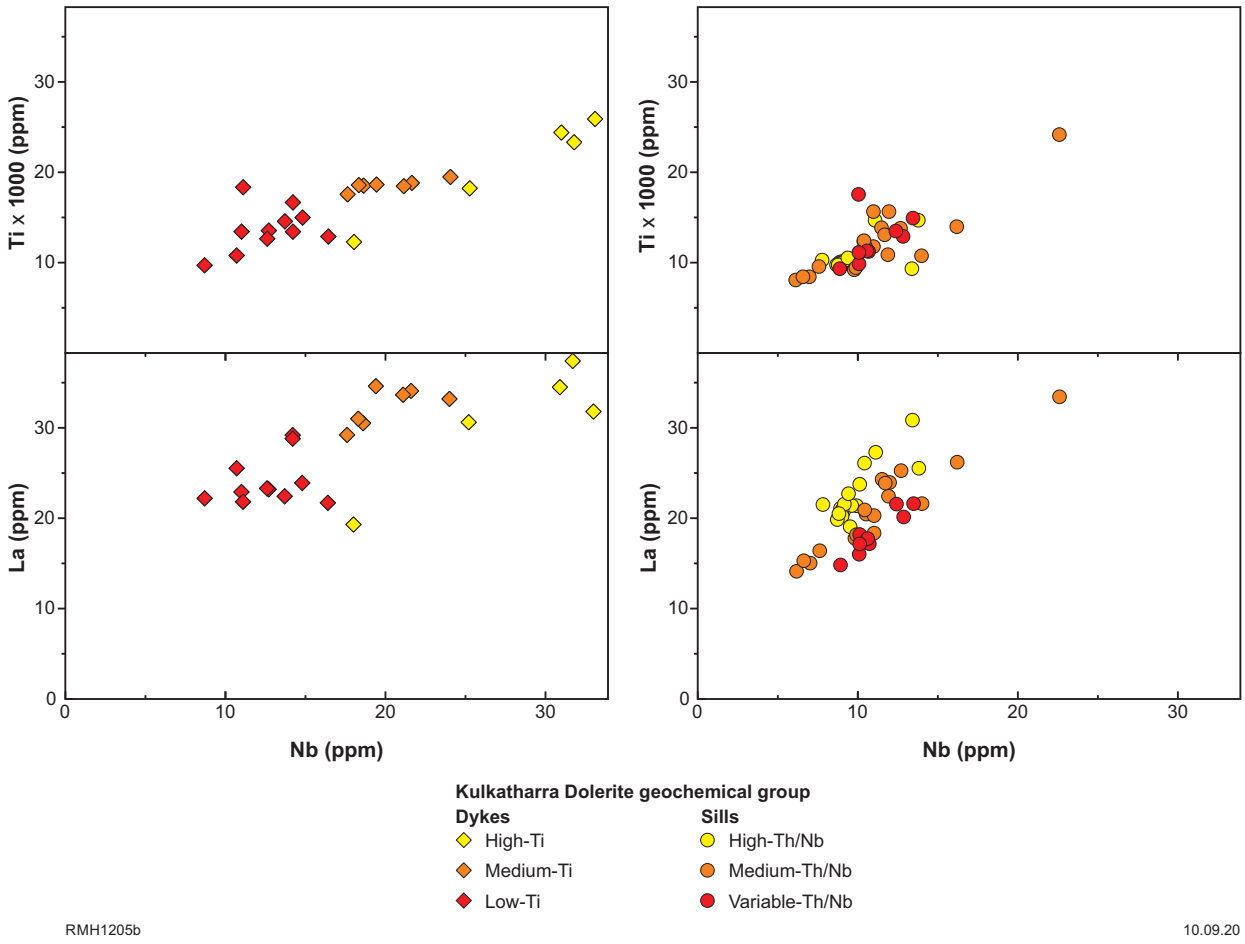

Figure 19. continued

corresponds with the petrographically determined Type 1 dolerites described earlier and the Low-Ti dykes to the southeast correspond to the Type 2 dolerites.

Sm–Nd isotopes and potential magma sources

Kulkatharra Dolerite dykes have relatively high $^{143}Nd/^{144}Nd_{(i)}$ values of 0.510796 to 0.511289 (calculated at 1075 Ma), and a wide range of $\varepsilon_{Nd(i)}$ values between 0.82 and –8.82 (Fig. 14, Table 2). Two-stage DM Nd model ages (T_{DM}^{2}) range from 2.34 to 1.62 Ga, although most are close to 1.7 Ga. Low $\varepsilon_{Nd(i)}$ values of –3.87 to –8.82 for three samples suggest at least local influence of evolved crustal material (Table 2). These three samples account for most of the observed isotopic variation within the sampled Kulkatharra dykes, and were collected from within or marginal to exposed Capricorn Group sedimentary rocks of the Ashburton Basin and it is possible that this host rock, at least locally, was more easily incorporated (i.e. assimilated) into the intruding mafic dykes. Sample GSWA 143497 contained inherited zircons dated at 2988–1707 Ma, indicating incorporation of older rocks (GSWA 206949, Lu et al., 2017). Disregarding the three non-radiogenic samples, the remaining samples include four Medium-Ti group samples geochemically equivalent to Type 1 dolerites and four samples of Type 2 dolerites (see Petrography section above and Appendix 2). These samples are almost isotopically equivalent, the Type 1 dolerites having $\varepsilon_{Nd(i)}$ marginally <0, the Type 2 dolerites typically having $\varepsilon_{Nd(i)}$ marginally >0. This, albeit slight, isotopic difference is consistent with the observed trace element differences between the various dyke populations in reflecting slight variations in bulk source compositions.

As with the Minga dykes, the Nd isotope composition of the mantle source for the Kulkatharra dykes lay between DM and CHUR, based on the Nd isotope composition of the most radiogenic sample (Fig. 14). However, trace element data, particularly the low Nb/La and high-Th/Nb ratios (Fig. 15), also require a crustal component within the bulk source, likely a greater mass component than was present within the source for the Minga dykes. An exception here is the High-Ti group (no Nd isotope data available), which has the highest Nb/La ratio (Fig. 19) (resulting in the least negative Nb anomaly on a primitive mantle-normalized trace element plot) (Fig. 11), suggesting only minimal crustal contamination. The High-Ti group also has trace element ratios more closely approaching values transitional between E-MORB and OIB than is the case for the other Kulkatharra dykes.

Apart from the three non-radiogenic dyke samples, the lack of any significant Nd isotope variation in the dykes over a significant variation in proxies of crustal contamination (Fig. 16) either suggests that any crustal contaminant was isotopically identical to mantle-derived magmas or that the mantle source was homogenously mixed with a crustal component prior to melt extraction. When plotted on a Th/Yb vs Nb/Yb discrimination diagram (Pearce, 2008; Fig. 21) the Kulkatharra dykes lie above the mantle array, many with Th/Nb ratios high enough to plot within the modern arc array (again, the High-Ti group is an exception, with Th/Nb values lying closer to the mantle array), but neither the samples as a group, nor the individual compositional subdivisions (i.e. Low-, Medium-, High-Ti) show any clear trend that can be interpreted in terms of crustal assimilation or melting of a subduction enriched source.

Comparison with Kulkatharra Dolerite sills

Kulkatharra Dolerite dykes are mainly quartz dolerite, moderately altered to unaltered, locally porphyritic, and some are enriched in Fe–Ti oxide minerals. Kulkatharra Dolerite sills are relatively unaltered, and medium to coarse grained away from chilled margins. The sills are typically quartz dolerite, locally (clinopyroxene and plagioclase) porphyritic, and locally contain coarse-grained to pegmatitic granophyric segregations in the central and upper parts of some sills.

Most dykes assigned to the Kulkatharra Dolerite are spatially associated with Kulkatharra sills (Blay et al., 2018c). Both dykes and sills are particularly extensive on the Pingandy Shelf, as well as within the core and along the northern limb of the Wanna Syncline on the Edmund, Mount Egerton, Collier, and Turee Creek 1:250 000 map sheets, although the dykes extend farther north than the sills, and intrude metasedimentary rocks of the Ashburton Basin (Fig. 2).

The mineralogy and major and trace element geochemistry of most Kulkatharra Dolerite sills and Type 2 Dolerite dykes is very similar (Table 3, Appendix 1; Blay et al., 2018c) – and is distinct from Type 1 Dolerite dykes, including the Medium-Ti dykes, as described above. However, where sills overlap the geographical range of Medium-Ti dykes, many of these sills themselves show slight enrichments in Ti, P and other incompatible trace elements (for example Nb) that characterize the Medium-Ti dykes. This suggests some form of genetic relationship either through a common enriched source or a common enriched crustal contaminant.

The Nd isotope range for the Kulkatharra sills ($\varepsilon_{Nd(i)}$ between 2.71 and –2.40, Table 2) overlaps the more radiogenic part of the range for the dykes. Disregarding the three very radiogenic dykes, the combined Nd isotope data for the sills and dykes show a trend to broadly decreasing $\varepsilon_{Nd(i)}$ values with increasing SiO_2 although correlations with other proxies for crustal contamination are less clear (Fig. 20).

On a Th/Yb vs Nb/Yb discrimination diagram (Pearce, 2008; Fig. 21), the Kulkatharra Dolerite sills separate into two groups each forming Th/Yb vs Nb/Yb trends that parallel the mantle array at distinct but high-Th/Nb ratios within the modern arc array. A third group shows a distinct contrasting trend to higher Th/Yb ratios and constant Nb/Yb. The two trends that parallel the modern arc array (High-Th/Nb trend and Medium-Th/Nb trend) are typical of rocks formed through partial melting of subducted modified mantle sources. The rocks defining these trends are separated here into High-Th/Nb and Medium-Th/Nb groups (Figs 18, 19, 21). The third trend is typical of rocks (Variable-Th/Nb group) formed by progressive assimilation of crust into a mantle-derived magma during magma ascent. When the two arc-like groups are plotted spatially, they broadly correspond to two east-southeasterly trending bands with minimal overlap, which together show a broadly south-southwesterly decrease in Th/Nb. If this trend is valid then it might reflect a systematic south-southwesterly decrease in the extent to which the mantle source for the sills was previously metasomatized. Because there is no evidence that subduction processes were in operation within the region at or around the time of Kulkatharra magmatism, the metasomatized mantle source might represent a fossil mantle wedge, with a suture to the northeast.

Summary

Most dykes assigned to the c. 1075 Ma Kulkatharra Dolerite are spatially associated with Kulkatharra sills, and dykes and sills are similar both mineralogically and geochemically, suggesting that the dykes may have acted as feeders for the sills. Type 1 dykes are fine grained, porphyritic, and enriched in titanomagnetite and/or ilmenite. Type 2 dykes are mainly northeasterly and easterly trending, fine to medium grained, subophitic, rarely porphyritic, and locally epidotized. Kulkatharra Dolerite dykes have high V, relatively low Cr and Ni, and are enriched in REE (particularly LREE) and HFSE (principally Ti, Nb and Zr). Mantle-normalized trace element patterns have negative slopes and typically show moderate negative Nb anomalies. The samples with lowest negative Nb anomalies (High-Ti group) are also the most trace element enriched rocks and their trace element characteristics suggest that they are only very weakly contaminated by crustal material, and that their primary compositions approximated something transitional between E-MORB and OIB. For the remainder of the dykes and sills, the moderately negative Nb anomalies, combined with Nd isotope compositions close to, or less radiogenic than CHUR, indicate a crustal component within the bulk source. Three samples, in particular, show significant evidence for incorporation of evolved crust and these samples account for most of the observed Nd isotopic variation within the Kulkatharra Dolerite. All three were sampled from within or marginal to exposed Capricorn Group sedimentary rocks of the Ashburton Basin and it is possible that this host rock, at least locally, was more easily incorporated into the intruding mafic dykes.

Dykes and sills can be divided into groups based on subtle compositional variations (e.g. High-, Medium-, Low-Ti and High-, Medium- and Variable-Th/Nb) and these groups are broadly spatially restricted. The compositions of some of the Low-Ti group dykes can be reconciled against that of the sills to which they are most closely associated spatially.

Table 3. Major oxides and trace elements in dolerite sill samples

	Waldburg sills		*Narimbunna sills*		*Kulkatharra sills*	
	Average	*Range*	*Average*	*Range*	*Average*	*Range*
Oxides			*Percentage (wt%)*			
SiO_2	48.85	47.93 – 49.69	49.49	46.74 – 51.28	50.81	44.47 – 54.6
TiO_2	1.47	1.00 – 1.68	1.60	0.85 – 2.49	2.02	1.34 – 4.04
Al_2O_3	13.76	11.99 – 14.65	13.80	12.43 – 16.39	13.21	11.30 – 14.46
$*Fe_2O_3^T$	13.25	11.60 – 14.20	13.28	9.96 – 16.76	14.54	10.99 – 18.33
MnO	0.20	0.18 – 0.22	0.23	0.16 – 0.63	0.19	0.16 – 0.23
MgO	7.06	6.23 – 9.85	6.17	4.46 – 8.51	5.09	3.22 – 9.74
CaO	10.89	10.18 – 11.62	9.68	4.95 – 12.34	8.95	7.15 – 11.56
Na_2O	2.16	1.75 – 2.48	2.12	1.23 – 3.65	2.43	1.63 – 3.19
K_2O	0.39	0.28 – 0.47	0.89	0.32 – 2.33	1.12	0.37 – 1.96
P_2O_5	0.13	0.08 – 0.14	0.21	0.11 – 0.62	0.23	0.14 – 0.40
Elements			*Parts per million (ppm)*			
Cr	227	134–348	150	16–542	85	8.0–759
Ni	95	69–148	76	22–152	100	50–245
V	324	275–366	323	226–443	350	140–897
Pb	2.3	0.7– 6.0	3.4	0.6 – 15.8	7.6	3.4 – 13.0
Cu	90	71–109	98	46–144	168	48–351
La	7.21	4.87 – 8.30	15.98	7.97 – 29.51	21.6	14.09 – 31.90
Ce	17.06	11.40 – 19.40	33.41	16.70 – 60.05	46.94	31.02 – 72.30
Pr	2.46	1.65 – 2.85	4.25	2.17 – 7.48	5.95	3.74 – 9.50
Nd	11.86	8.02 – 13.80	18.51	9.62 – 30.65	26.15	17.75 – 42.05
Sm	3.37	2.42 – 4.03	4.33	2.43 – 7.22	6.24	4.18 – 10.05
Eu	1.23	0.99 – 1.36	1.52	0.84 – 2.62	1.92	1.29 – 3.02
Gd	3.96	2.94 – 4.73	4.55	2.34 – 8.07	6.53	4.50 – 10.15
Tb	0.64	0.48 – 0.72	0.75	0.38 – 1.32	1.07	0.70 – 1.67
Dy	4.05	3.08 – 4.64	4.54	2.48 – 7.80	6.14	3.96 – 9.40
Ho	0.85	0.65 – 0.98	0.96	0.50 – 1.42	1.25	0.79 – 1.95
Er	2.32	1.78 – 2.60	2.68	1.57 – 4.66	3.30	2.03 – 4.74
Yb	2.05	1.51 – 2.51	2.45	1.33 – 4.03	2.85	1.83 – 4.21
Lu	0.32	0.23 – 0.36	0.38	0.20 – 0.60	0.43	0.27 – 0.68
Y	22.6	17.6 – 25.9	27.0	15.0 – 41.4	34.6	21.8 – 56.7
Zr	79	55–93	119	54 – 331	176	99–290
Nb	5.3	3.7 – 6.4	10.1	4.80 – 18.8	11.5	6.25 – 26.0
Hf	2.30	1.46 – 2.80	3.04	1.50 – 7.20	4.69	2.82 – 8.30
Th	0.78	0.60 – 0.94	1.88	0.90 – 3.90	4.88	2.68 – 8.47
U	0.16	0.12 – 0.19	0.38	0.17 – 0.80	0.69	0.34 – 1.16
Ti	8840	6019–10072	9606	5084–14904	12091	8034–18825
Ta	0.34	0.22 – 0.40	0.61	0.29 – 1.20	0.67	0.39 – 1.40
Sc	39.4	37.0 – 43.0	36.2	28.0 – 43.6	29.0	25.0 – 36.0
Ga	19.5	14.7 – 21.7	19.00	15.1 – 23.2	22.2	15.7 – 26.7

NOTE: *All Fe as Fe_2O_3

For example, most Low-Ti group dykes spatially associated with High-Th/Nb sills also have high-Th/Nb ratios similar to those sills.

Many of the sills fall into one of three groups defined by distinct trends in Th/Yb vs Nb/Yb space (Fig. 21). Two groups with Th/Nb values within and parallel to the modern arc arrays can be interpreted as derived from an already enriched (metasomatized) and homogenized mantle source. It can further be speculated that the trend of decreasing Th/Nb to the south-southwest maps out similar compositional changes within a potential fossil mantle wedge, and requires the fossil suture to lie to the northeast. The third group of sills, the Variable-Th/Nb, shows a trend (Fig. 21) that suggests progressive crustal assimilation during emplacement has dominated compositional evolution – potentially overprinting compositional features more directly attributable to the mantle source composition.

Mundine Well Dolerite dykes

Field observations

Most dolerite dykes in the western Capricorn Orogen that trend north to northeast are assigned to the c. 755 Ma Mundine Well Dolerite (Hickman and Lipple, 1975; Wingate and Giddings, 2000). Mundine Well dykes form an arcuate swarm that extends from the southern Gascoyne Province to the northern Pilbara Craton (Wingate and Giddings, 2000; Wingate, 2002; Wingate and Blay, 2020; Fig. 1). The Mundine Well dykes are not metamorphosed and represent the last known mafic igneous event in the Capricorn Orogen (Wingate and Giddings, 2000; Martin et al., 2005). Within the study area, Mundine Well dykes are concentrated mainly on Mangaroon and Maroonah (Fig. 2), where they intrude Neoarchean–Paleoproterozoic rocks of the Gascoyne Province, Paleoproterozoic to Mesoproterozoic sedimentary rocks of the Edmund Basin, and Mesoproterozoic sedimentary rocks of the Collier Basin. Farther north, the dykes cut Paleoproterozoic metasedimentary rocks of the Ashburton and Blair Basins. These dykes also intrude sills of the Waldburg, Narimbunna and Kulkatharra Dolerites (Morris and Pirajno, 2005; Blay et al., 2018c). No dolerite sills with chemistry similar to that of the Mundine Well dykes have been identified anywhere in the Capricorn Orogen, and it is not known if the Mundine Well magmas were ever emplaced as high-level sills or volcanic rocks that have since been removed by erosion. The Mundine Well dykes are less extensive farther to the east, being mainly confined to the western parts of Ullawarra and Edmund (Fig. 2), where they trend mainly northeast. This is similar to the trend of Kulkatharra Dolerite dykes in this area, making it difficult to distinguish between the suites based on orientation alone.

Mundine Well dykes have strike lengths up to 75 km and are mostly 5–30 m wide, although some dykes are up to 200 m wide. Thin dykes are typically exposed as patchy trains of weathered cobbles and boulders, whereas along the margins of some thicker dykes there are spectacular ridges of contact-metamorphosed granite (e.g. OXBEDM000206, 365239E 7367348N). Chilled dyke margins are typically aphanitic to fine grained. Thinner dykes are composed of fine- to medium-grained dolerite, and are either aphyric or weakly porphyritic, with up to 5% tabular plagioclase phenocrysts <10 mm long. The central parts of some thicker dykes are locally composed of coarse-grained to pegmatitic leucogabbro. Mundine Well dykes locally exhibit weak, pervasive epidotization (disseminated or in veinlets), and rarely exhibit intense epidote–sericite±quartz alteration accompanied by bleaching in adjacent host rocks (e.g. SXSMAN5915, 365320E 7367700N; SXSMAN6121, 349260E 7355550N).

Some thick Mundine Well dykes have melted their host rocks during emplacement (Wingate and Giddings, 2000), producing hornfelsed zones up to 50 m wide (e.g. SXSMAN6227, 359320E 7373390N; SXSMAN6143, 357930E 7349610N, and SXSMAN6226, 359300E 7373140N). Some dykes are locally contaminated with abundant xenoliths of granitic country rock (Wingate and Giddings, 2000; Martin et al., 2005; Li et al., 2006; Wingate and Blay, 2020). One of these dykes, located about 1.3 km west of Alma Well on Mangaroon, consists of heterogeneous quartz diorite to granodiorite that contains partly resorbed K-feldspar xenocrysts, about 15% rounded quartz xenocrysts with biotite-rich rims, granophyre, and rounded to subangular dolerite inclusions (e.g. SXSMAN6095, 351680E 7359790N and AMTBAN002807, 355199E 7351777N). Some dolerite inclusions contain acicular apatite crystals, which commonly develop in quenched mafic magma (e.g. Vernon, 1983). Collectively, these features suggest mingling and limited hybridization between mafic and felsic magmas, the latter possibly derived from melting of wallrocks during dolerite intrusion (Wingate and Giddings, 2000). On Mangaroon and Maroonah, some dykes contain inclusions of quartz diorite, syenite, tonalite, and biotite monzogranite, suggesting dyke intrusion into active faults.

Petrography

Although not metamorphosed, some Mundine Well Dolerite dykes are locally strongly weathered or hydrothermally altered. They commonly exhibit intergranular to subophitic textures and are locally micrographic. Mundine Well dykes include both granophyric quartz-normative and olivine-normative varieties (Appendix 2 Fig. 2.19; Wingate and Giddings, 2000). Both varieties contain clinopyroxene and/or orthopyroxene and quartz–feldspar granophyre (Wingate, 2003; Martin et al., 2005; Li et al., 2006). Plagioclase is anhedral to euhedral, clinopyroxene is equant and anhedral or prismatic, and interstitial quartz is anhedral to euhedral. Granophyric patches are typically interstitial to plagioclase. In olivine-bearing dykes, magnetite crystals partly enclose small plagioclase and/or orthopyroxene crystals. In some examples, orthopyroxene contains blebby augite lamellae, indicative of inverted pigeonite. Locally, Mundine Well dykes contain tabular crystals, possibly originally K-feldspar, completely pseudomorphed by clay minerals. Accessory minerals include biotite, opaque minerals, apatite, zircon, baddeleyite, and hornblende. Opaque minerals include magnetite, titanomagnetite, and rare pyrite, and commonly have euhedral and/or skeletal shapes and are intergrown with plagioclase, pyroxene, and biotite. Titanomagnetite locally shows exsolution textures and leucoxene alteration.

Very coarse-grained dolerite and/or leucogabbro in the centres of some thicker dykes (e.g. OXBPAL000005, 417672E 7497273N) is composed mainly of plagioclase, hornblende, and quartz. These rocks tend to be sampled preferentially for geochronology, because they commonly contain primary magmatic zircons (Wingate and Giddings, 2000). Locally, where dykes have assimilated granitic xenoliths, the dolerite is enriched in variably corroded and embayed quartz and feldspar, and xenocrystic zircons. These contaminated dolerites typically consist of a fine-grained groundmass of euhedral plagioclase and abundant interstitial quartz–feldspar granophyre. The groundmass may be altered to mainly chlorite, with minor amphibole, biotite, and epidote; feldspar xenocrysts may have montmorillonite and/or minor hematite alteration associated with weathering (Wingate and Giddings, 2000).

Secondary minerals in Mundine Well dykes include sericite, chlorite, amphibole, saussurite, and minor leucoxene, quartz, talc, epidote, prehnite, carbonate, and serpentine. Augite is commonly partially or completely overgrown by green–brown or pale green hornblende, which may also occur in fractures, or is partially altered to chlorite or biotite. Primary orthopyroxene is less abundant than clinopyroxene and is largely replaced by chlorite. Plagioclase is partially sericitized, especially along fractures, and may display minor epidotization. More extensive disseminated or veined epidote alteration is present in areas with a high density of mafic dykes (Martin et al., 2005).

Geochronology

Three northeasterly trending Mundine Well dykes have been dated directly using SHRIMP U–Pb baddeleyite and zircon geochronology. A 25 m-wide, northeasterly trending dyke, composed of medium- to coarse-grained quartz dolerite, about 3 km northwest of Glen Florrie homestead on Boolaloo, yielded a zircon age of 755 ± 3 Ma and a baddeleyite age of 757 ± 16 Ma (sample B7, Wingate and Giddings, 2000). Because baddeleyite inheritance in mafic rocks is extremely unlikely, the agreement between baddeleyite and zircon results indicates that the zircons formed during dyke crystallization, hence the more precise zircon age can be interpreted as an unambiguous age of emplacement (Wingate and Giddings, 2000). A poorly exposed, north-northeasterly trending dyke, consisting of medium- to coarse-grained olivine gabbro,

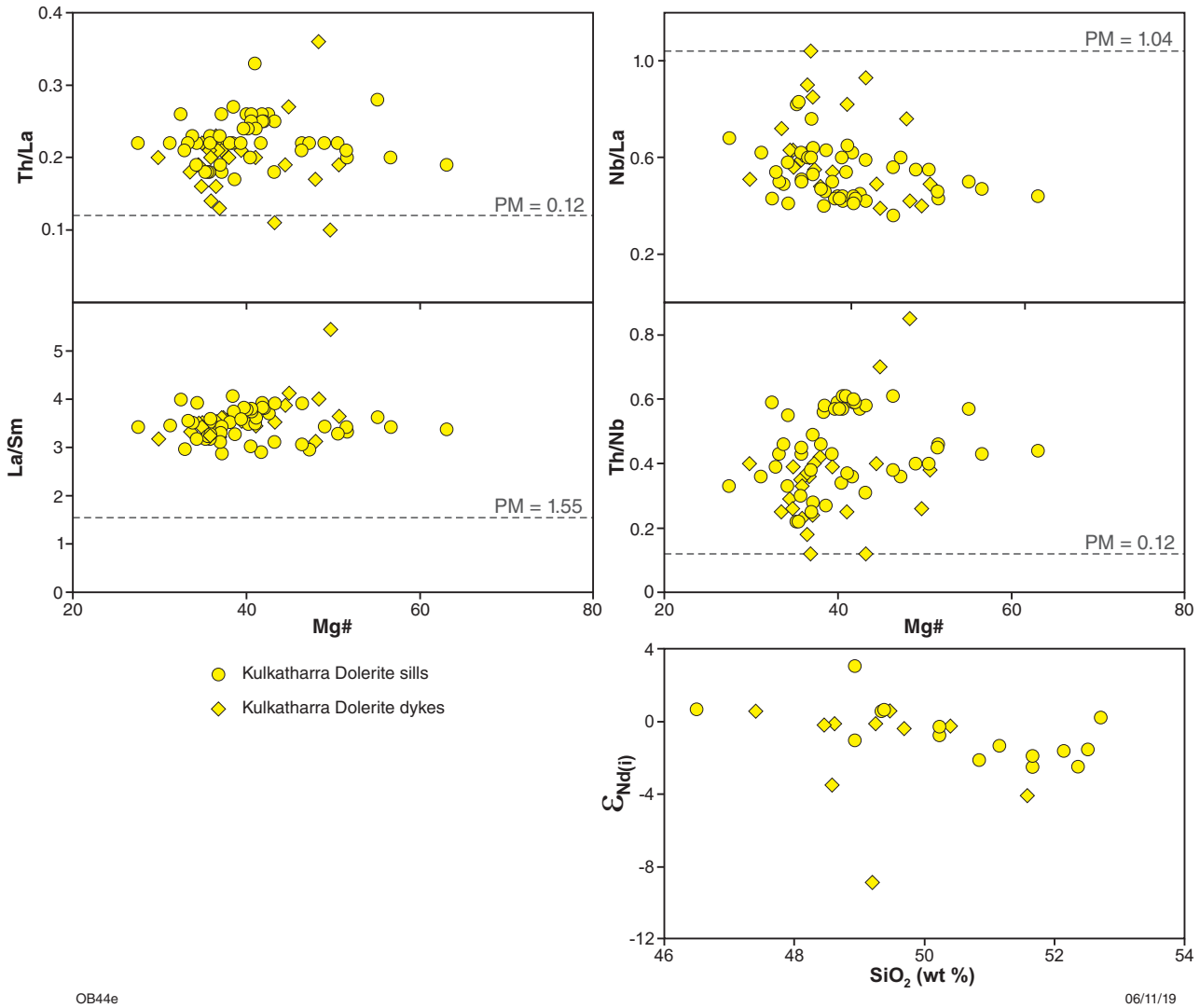

Figure 20. Binary variation diagrams for Kulkatharra Dolerite sills and dykes, showing variation of selected incompatible trace element ratios with Mg# and variation of $\varepsilon_{Nd(i)}$ with SiO_2. Mg# = molecular Mg/(Mg + total Fe) [values for PM (Sun and McDonough, 1989 – used for reference)]

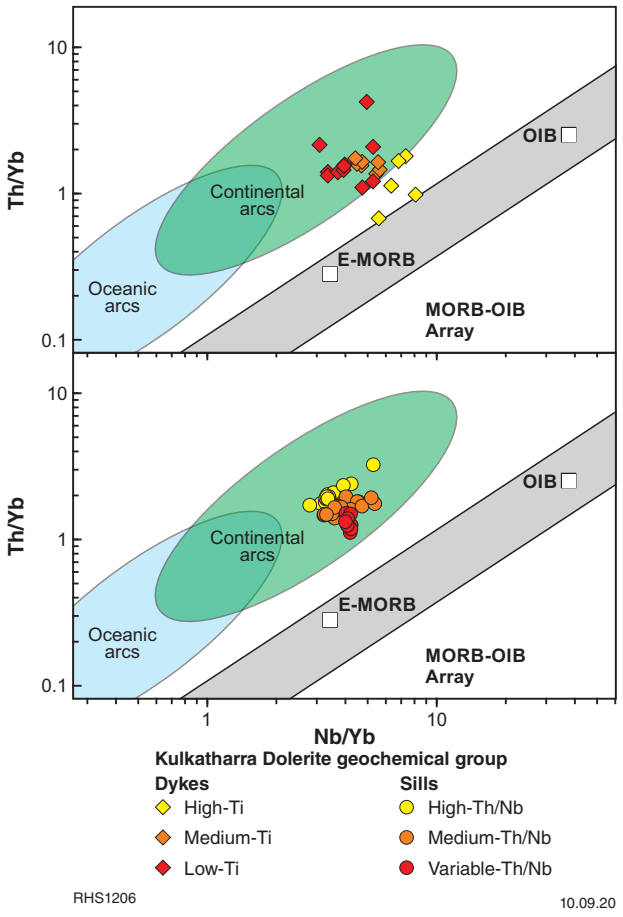

Figure 21. Th/Yb vs Nb/Yb discrimination diagrams (Pearce, 2008) for dykes and sills of Kulkatharra Dolerite. Although trends for the dykes are not clear, the diagram shows that the High- and Medium-Th/Nb sills each form an array at a constant Th/Nb ratio. Such arrays can be interpreted to reflect partial melting of a subduction-modified mantle source. The third group of sills, with Variable-Th/Nb, more likely reflects a mantle-derived magma that underwent more or less continuous assimilation of a high-Th 'crustal' component during emplacement. Abbreviations: E-MORB, enriched mid-oceanic ridge basalt; N-MORB, normal mid-oceanic ridge basalt; OIB, oceanic island basalt

about 2.5 km south of Joy Helen Mine on MAROONAH, provided a baddeleyite age of 748 ± 12 Ma (sample B6, Wingate and Giddings, 2000). A 15 m-wide, northeasterly trending dyke, composed of medium-grained, granophyric quartz dolerite, about 7.6 km north-northwest of Wyloo homestead, yielded a combined baddeleyite and zircon age of 753 ± 11 Ma (GSWA 206949) (Wingate et al., 2017b,c).

Geochemistry

Alteration

Mundine Well dykes are typically slightly altered, with an average LOI of about 1%, although volatile contents in some samples are up to 3.4% (Appendices 1, 5). Strong positive correlations of HFSE and REE with Zr indicate that their mobility was relatively unaffected by postmagmatic processes (Fig. 9). Most LILE elements, with the exception of Rb and Cs also show a reasonable to strong correlation with Zr, suggesting they too have not been significantly altered from primary concentrations (Appendix 3).

Major, trace, and rare earth element composition

Mundine Well Dolerite dykes can be classified as tholeiitic basalt (Fig. 10). The dykes exhibit a relatively wide range of major element oxide and trace element compositions (Table 1, Appendices 1, 5), including significant variation in SiO_2 (47–52%, average 50%), Na_2O (1.4 – 2.8%), and K_2O (0.6 – 1.6%), relatively high and highly variable MgO (3.4 – 12.6%,), generally high CaO (8.5 – 11.2%), and relatively low and highly variable TiO_2 (0.7 – 2.8%) and P_2O_5 (0.06 – 0.34%). These rocks are also distinguished by highly variable Cr (40–514 ppm, average 185 ppm) and moderate Ni (40–361 ppm, average 99 ppm) contents over a wide range of Mg# values from 33 to 71 (Table 1, Appendix 1).

Mantle-normalized trace element diagrams (Fig. 11) for the Mundine Well Dolerite show moderately to strongly fractionated trace element patterns with $(La/Yb)_N$ of 4.5 to 5.9 and have negative Nb anomalies of similar or greater scale to those seen in the Kulkatharra dykes (Fig. 11, Appendix 1). They exhibit high variation in REE and HFSE, for example La (8.7 – 25.6 ppm), Nd (9.8 – 29.5 ppm), Zr (57–201 ppm), Nb (3.3 – 17.2 ppm), and Ti (4041–16787 ppm) (Table 1). A positive correlation between Sc/V and Mg# (Fig. 12), together with a relatively wide range in Cr concentration (Table 1, Appendix 5), suggests fractional crystallization of clinopyroxene, whereas a decrease in Sr/Nd with increasing Zr suggests plagioclase fractionation, although not sufficient to result in a significant Eu anomaly (Fig. 11). The fractionated normalized trace element patterns reflect either or both low-degree melting of a mantle source or an evolved crustal component within the bulk source — the latter is required by the negative Nb anomalies.

Sm–Nd isotope analyses and potential magma sources

The Mundine Well Dolerite dykes have a range in $^{143}Nd/^{144}Nd_{(i)}$ from 0.511163 to 0.511694, with highly variable, predominantly negative $\varepsilon_{Nd(i)}$ values between 0.66 and –9.70, leading to DM two-stage Nd model ages (T_{DM}^2) ranging from 2.14 to 1.36 Ga (Table 2, Fig. 14). Based on the isotopic composition of the most radiogenic sample, the dolerite dykes were most likely derived from a source with a composition between depleted and chondritic mantle (Fig. 14) but which interacted with relatively large amounts of highly evolved, old crustal material. There are numerous examples in outcrop of Mundine Well dykes that contain abundant granitic xenoliths, as described above. A positive correlation between $\varepsilon_{Nd(i)}$ and Nb/La, and negative correlations between $\varepsilon_{Nd(i)}$ and both SiO_2 and La/Sm (Fig. 16) also suggest relatively high crustal contamination and/or significant heterogeneity in mantle source composition.

Summary

The Mundine Well Dolerite consists only of dolerite dykes, and no related sills have been identified within the Capricorn Orogen. The dykes are composed mainly of medium- to coarse-grained dolerite, although some are locally contaminated by granitic material, and generally trend north to northeast, and less commonly north-northwest (Fig. 2). Wallrocks were locally melted during dyke emplacement producing intensely hornfelsed zones. Most Mundine Well dykes are only slightly altered and consist of quartz- or olivine-normative dolerite, in which the main minerals are plagioclase, clinopyroxene and/or orthopyroxene, and minor quartz–feldspar granophyre. The Mundine Well dykes are tholeiitic and exhibit highly variable Cr contents (40–514 ppm) over a wide range of Mg#, from 33 to 71 (Fig. 12). Mantle-normalized trace element patterns (Fig. 11) feature distinct moderately to strongly fractionated REE compositions and negative Nb anomalies. Their chemistry is consistent with low-degree partial melting from a mantle source and their primary composition might have approximated those of E-MORB, based on similar Nb/Yb ratios (Fig. 13). Nevertheless, outcrop observations, and geochemical proxies for crustal contamination, indicate crustal contamination and this is also required by the negative Nb anomalies. Vertical arrays in the Th/Yb vs Nb/Yb diagram (Fig. 13; Pearce and Peate, 1995; Pearce, 2008) also suggest a crustal contribution to the bulk source and indicate this was added to a magma of broadly E-MORB composition, via contamination during magma accent rather than a subduction contribution to the mantle source.

Conclusions

Field observations, petrography, geochronology, geochemistry, and isotope data for dolerite dykes and sills in the western Capricorn Orogen are combined to explore possible relationships between these intrusions. Prior to this study, dolerite dykes other than those of the c. 755 Ma Mundine Well Dolerite had not been studied systematically and were not assigned to particular rock units. Dolerite dykes have been distinguished that are related to the 1083–1075 Ma Kulkatharra Dolerite, a unit previously defined on the basis of dolerite sills alone. An areally restricted swarm of non-dated dolerite dykes, named here the Minga Dolerite, was thought initially to be related to sills of the 1465–1450 Ma Narimbunna Dolerite, based on cursory similarities in petrography and geochemistry. However, our detailed analysis of geochemical and isotope data indicates that the Minga Dolerite and Narimbunna Dolerite are not related.

Minga Dolerite dykes trend mainly north-northwesterly, and typically consist of strongly altered, melanocratic dolerite. Although they have alteration and cursory geochemical similarities with Narimbunna Dolerite sills, they are not spatially associated with sills. Together with distinctive Nd isotope compositions, our geochemical data suggest that the dykes and sills almost certainly formed independently from each other, from compositionally distinctive source rocks and through contrasting petrogenetic processes. The Minga dykes represent mantle-derived magmas, possibly with compositions resembling E-MORB that were more or less continuously contaminated through assimilation of crustal material during emplacement. The Narimbunna Dolerite sills formed through remelting of a previously subduction-modified mantle source, and underwent more or less closed-system compositional evolution during emplacement.

Most dykes assigned to the 1083–1075 Ma Kulkatharra Dolerite are spatially associated with Kulkatharra sills. The dykes and sills are similar both mineralogically and geochemically, suggesting that the dykes acted as feeders for the sills. This is supported by U–Pb dates of c. 1081 for a single zircon in one dyke, and c. 1069 Ma for a single zircon in the contact aureole of another dyke. Discrete and broadly spatially restricted groups of Kulkatharra dykes can be recognized based on combinations of mineralogy, geochemistry and Nd isotope compositions; these groups include High-, Medium-, and Low-Ti and High-, Medium-, and Variable-Th/Nb. Some Low-Ti group dykes have compositions similar to those of the sills to which they are most closely associated spatially. For example, most Low-Ti dykes that are spatially associated with High-Th/Nb sills also have High-Th/Nb ratios similar to the sills. Two groups with Th/Nb values similar to those of modern arc arrays may have been derived from a metasomatized and homogenized mantle source, and a trend of decreasing Th/Nb to the south-southwest maps out compositional changes within a potential fossil mantle wedge. The third group of Kulkatharra sills, the Variable-Th/Nb group, exhibits a trend that suggests that compositional evolution was dominated by progressive crustal assimilation during emplacement.

The c. 755 Ma Mundine Well Dolerite consists mainly of north- to northeasterly trending, medium- to coarse-grained, quartz- or olivine-normative dykes, and no Mundine Well sills are known. Their chemistry is consistent with low-degree partial melting from a mantle source and their primary composition might have approximated those of E-MORB, based on similar Nb/Yb ratios. However, observations of abundant granitic xenoliths in some outcrops, together with geochemical proxies for contamination and negative Nb anomalies, clearly indicate crustal contamination. Vertical arrays in a Th/Yb vs Nb/Yb diagram also imply a crustal contribution to the bulk source and suggest this was added to a magma of broadly E-MORB composition, via contamination during magma ascent rather than a subduction contribution to the mantle source.

References

Bea, B, Montero, P and Ortega, M 2006, A LA-ICP-MS evaluation of Zr reservoirs in common crustal rocks: Implications for Zr and Hf geochemistry, and zircon-forming processes: The Canadian Mineralogist, v. 44, p. 693–714.

Bingen, B, Austrheim, H and Westinghouse, M 2001, Ilmenite as a source for zirconium during high-grade metamorphism? Textural evidence from the Caledonides of western Norway and implications for zircon geochronology: Petrology, v. 42, p. 355–375.

Blay, OA, Johnson, SP and Thorne, AM 2020, Narimbunna Dolerite (P_-_nr-od): Geological Survey of Western Australia; WA Geology Online, Explanatory Notes extract, accessed 4 June 2020, <www.dmirs.wa.gov.au/ens>.

Blay, OA, Johnson, SP, Thorne, AM and Cutten, HN 2018a, Waldburg Dolerite (P_-_wa-od): Geological Survey of Western Australia; WA Geology Online, Explanatory Notes extract, accessed 4 June 2020, <www.dmirs.wa.gov.au/ens>.

Blay, OA, Johnson, SP, Wingate, MTD and Thorne, AM 2018b, Kulkatharra Dolerite (P_-WKku-od): Geological Survey of Western Australia; WA Geology Online, Explanatory Notes extract, accessed 4 June 2020, <www.dmirs.wa.gov.au/ens>.

Blay, OA, Johnson, SP, Wingate, MTD, Thorne, AM, Kirkland, CL, Tessalina, SG and Cutten, HN 2018c, A new Mesoproterozoic mafic intrusive event in the Capricorn Orogen: Geological Survey of Western Australia, Record 2018/4, 41p.

Blundy, I and Wood, B 2003, Partitioning of trace elements between crystals and melts: Earth and Planetary Science Letters, v. 210, p. 383–397.

Bouvier, A, Vervoort, JD and Patchett, PJ 2008, The Lu–Hf and Sm–Nd isotopic composition of CHUR: constraints from unequilibrated chondrites and implications for the bulk composition of terrestrial planets: Earth and Planetary Science Letters, v. 273, no. 1–2, p. 48–57, doi:10.1016/j.epsl.2008.06.010.

Cann, JR 1970, Rb, Sr, Y, Zr, and Nb in some ocean floor basaltic rocks: Earth and Planetary Science Letters, v. 10, no. 1, p. 7–11.

Cawood, PA and Tyler, IM 2004, Assembling and reactivating the Proterozoic Capricorn Orogen: Lithotectonic elements, orogenies, and significance: Precambrian Research, v. 128, p. 201–218.

Champion, DC and Huston, DL 2016, Radiogenic isotopes, ore deposits and metallogenic terranes: Novel approaches based on regional isotopic maps and the mineral systems concept: Ore Geology Reviews, v. 76, p. 229–256, doi:10.1016/j.oregeorev.2015.09.025.

Cutten, HN, Johnson, SP, Thorne, AM, Wingate, MTD, Kirkland, CL, Belousova, EA, Blay, OA and Zwingmann, H 2016, Deposition, provenance, inversion history and mineralization of the Proterozoic Edmund and Collier Basins, Capricorn Orogen: Geological Survey of Western Australia, Report 127, 74p.

Cutten, HNC and Johnson, SP 2018, Kuparr Tectonic Event (KU): WA Geology Online, Explanatory Notes extract: Geological Survey of Western Australia, accessed 13 November 2019, <www.dmirs.wa.gov.au/ens>.

Daniels, JL 1968, Edmund, WA Sheet SF50-14: Geological Survey of Western Australia, 1:250 000 Geological Series.

Ernst, RE and Buchan, KL 2001, Mantle plumes: Their identification through time: Geological Society of America, Special Paper 352, 593p.

Gélinas, L, Mellinger, M and Trudel, P 1982, Archean mafic metavolcanics from the Rouyn-Noranda district, Abitibi Greenstone Belt, Quebec.1. Mobility of the major elements: Candian Journal of Earth Sciences, v. 19, p. 2258–2275.

Geological Survey of Western Australia 2020, GeoChem Extract: Western Australian Geochemistry (WACHEM) database: Geological Survey of Western Australia, accessed 4 June 2020, <www.dmirs.wa.gov.au/launch/geochemistry>.

Gladkochub, DP, Donskaya, TV, Wingate, MTD, Mazukabzov, AM, Pisarevsky, SA and Kornilova, TA 2013, Using the isotope dating of endocontact hybrid rocks for the age determination of mafic rocks (southern Siberian craton): Russian Geology and Geophysics, v. 54, p. 1340–1351.

Halls, HC 1982, The importance and potential of mafic dyke swarms in studies of geodynamic processes: Geoscience Canada, v. 9, no. 3, p. 145–154.

Halls, HC and Zhang, B 1995, Tectonic implications of clouded feldspar in Proterozoic mafic dykes, *in* Geological Society of India Memoir *edited by* TC Devaraju, Dyke swarms of Peninsula India, p. 65–80.

Halls, HC and Zhang, B 1998, Uplift structure of the southern Kapuskasing zone from 2.45 Ga dike swarm displacement, v. 26, no. 1, p. 67–70, doi:10.1130/0091-7613(1998)026%3C0067:USOTSK%3E2.3.CO;2.

Haluzova, E, Ackerman, L, Pasava, J, Jonasova, S, Svojtka, M, Hrstka, T and Veselovsky, F 2015, Geochronology and characteristics of Ni-Cu-(PGE) mineralization ar Rozany, Lusatian Granitoid Complex, Czech Republic: Journal of Geosciences, v. 60, p. 219–236, doi:10.3190/jgeosci.204.

Hickman, AH and Lipple, SL 1975, Explanatory notes on the Marble Bar 1:250 000 Geological Series map sheet, Western Australia: Geological Survey of Western Australia, Record 1974/20, 90p.

Howard, HM, Smithies, RH, Evins, PM, Kirkland, CL, Werner, M and Wingate, MTD 2019, Warakurna Supersuite (P_-WK-xo-f): Geological Survey of Western Australia; WA Geology Online, Explanatory Notes extract, accessed 4 June 2020, <www.dmirs.wa.gov.au/ens>.

Howard, HM, Smithies, RH and Pirajno, F 2007, Geochemical and Nd isotopic signatures of mafic dykes in the western Musgrave Complex, *in* Geological Survey of Western Australia Annual Review 2005-06: Geological Survey of Western Australia, p. 64–71.

Humbert, F, Kock, MO de, Altermann, W, Elburg, MA, Lenhardt, N, Smith, AJB and Masango, S 2018, Petrology, physical volcanology and geochemistry of a Paleoproterozoic large igneous province: the Hekpoort Formation in the southern Transvaal sub-basin (Kaapvaal craton): Precambrain Research, v. 315, p. 232–256, doi:10.1016/j.precamres.2018.07.022.

Hynes, A 1980, Carbonatization and mobility of Ti, Y, and Zr in Ascot Formation metabasalts, SE Quebec: Contributions to Mineralogy and Petrology, v. 75, p. 79–87.

Irvine, TN and Baragar, WRA 1971, A guide to the chemical classification of the common volcanic rocks: Canadian Journal of Earth Sciences, v. 8, p. 523–548.

Johnson, SP, Korhonen, FJ, Kirkland, CL, Cliff, J, Belousova, EA and Sheppard, S 2017a, Crustal differentiation in the Proterozoic Capricorn Orogen: Geological Survey of Western Australia, Report 168, 22p.

Johnson, SP, Korhonen, FJ, Kirkland, CL, Cliff, JB, Belousova, EA and Sheppard, S 2017b, An isotopic perspective on growth and differentiation of Proterozoic orogenic crust: From subduction magmatism to cratonization: Lithos, 268–271, p. 76–86.

Johnson, SP, Sheppard, S, Rasmussen, B, Wingate, MTD, Kirkland, CL, Muhling, JR, Fletcher, IR and Belousova, E 2010, The Glenburgh Orogeny as a record of Paleoproterozoic continent-continent collision: Geological Survey of Western Australia, Record 2010/5, 54p.

Johnson, SP, Sheppard, S, Rasmussen, B, Wingate, MTD, Kirkland, CL, Muhling, JR, Fletcher, IR and Belousova, EA 2011, Two collisions, two sutures: Punctuated pre-1950 Ma assembly of the West Australian Craton during the Ophthalmian and Glenburgh Orogenies: Precambrian Research, v. 189, no. 3-4, p. 239–262, doi:10.1016/j.precamres.2011.07.011.

Johnson, SP, Thorne, AM, Tyler, IM, Korsch, RJ, Kennett, BLN, Cutten, HN, Goodwin, J, Blay, OA, Blewett, RS, Joly, A, Dentith, MC, Aitken, ARA, Holzschuh, J, Salmon, M, Reading, A, Heinson, G, Boren, G, Ross, J, Costelloe, RD and Fomin, T 2013, Crustal architecture of the Capricorn Orogen, Western Australia and associated metallogeny: Australian Journal of Earth Sciences, v. 60, no. 6–7, p. 681–705, doi:10.1080/08120099.2013.826735.

Kirkland, CL, Spaggiari, CV, Pawley, MJ, Wingate, MTD, Smithies, RH, Howard, HM, Tyler, IM, Belousova, EA and Poujol, M 2011, On the edge: U-Pb, Lu-Hf, and Sm-Nd data suggests reworking of the Yilgarn Craton margin during formation of the Albany-Fraser Orogen: Precambrian Research, v. 187, p. 223–247.

Korhonen, FJ, Johnson, SP, Wingate, MTD, Kirkland, CL, Fletcher, IR, Dunkley, DJ, Roberts, MP, Sheppard, S, Muhling, JR and Rasmussen, B 2017, Radiogenic heating and craton-margin plate stresses as drivers for intraplate orogeny: Journal of Metamorphic Geology, v. 35, no. 6, p. 631–661, doi:10.1111/jmg.12249.

Kretz, R 2003, Dendritic magnetite and ilmenite in 590 Ma Grenville dikes near Otter Lake, Quebec, Canada: Canadian Mineralogist, v. 41, p. 1049–1959.

Li, X-H, Li, Z-X, Wingate, MTD, Chung, S-L, Liu, Y, Lin, G-C and Li, W-X 2006, Geochemistry of the 755 Ma Mundine Well dyke swarm, northwestern Australia: Part of a Neoproterozoic mantle superplume beneath Rodinia? Precambrian Research, v. 146, no. 1–2, p. 1–15, doi:10.1016/j.precamres.2005.12.007.

Lu, Y, Wingate, MTD, Kirkland, CL and Cutten, HN 2017, 143497: dolerite dyke, ESR Well No. 12; Geochronology Record 1421: Geological Survey of Western Australia, 4p.

Ludden, J, Gélinas, L and Trudel, P 1982, Archaean metavolcanics from the Rouyn-Noranda district, Abitibi greenstone belt, Quebec. 2. Mobility of trace elements and petrogenetic constraints: Canadian Journal of Earth Sciences, v. 19, p. 2276–2287.

Lugmair, GW and Marti, K 1978, Lunar initial $^{143}Nd/^{144}Nd$: differential evolution of the lunar crust and mantle: Earth and Planetary Science Letters, v. 39, p. 349–357.

Martin, DMcB, Sheppard, S and Thorne, AM 2005, Geology of the Maroonah, Ullawarra, Capricorn, Mangaroon, Edmund, and Elliott Creek 1:100 000 sheets: Geological Survey of Western Australia, 1:100 000 Geological Series Explanatory Notes, 65p.

Martin, DMcB, Sheppard, S, Thorne, AM, Farrell, TR and Groenewald, PB 2007, Proterozoic geology of the western Capricorn Orogen — a field guide: Geological Survey of Western Australia, Record 2006/18, 43p.

Martin, DMcB, Sircombe, KN, Thorne, AM, Cawood, PA and Nemchin, AA 2008, Provenance history of the Bangemall Supergroup and implications for the Mesoproterozoic paleogeography of the West Australian Craton, *in* Assembling Australia: Proterozoic building of a continent *edited by* PA Cawood and RJ Korsch, Precambrian Research 166, p. 93–110.

Martin, DMcB and Thorne, AM 2004, Tectonic setting and basin evolution of the Bangemall Supergroup in the northwestern Capricorn Orogen: Precambrian Research, v. 128, no. 3-4, p. 385–409.

Morris, PA and Pirajno, F 2005, Mesoproterozoic sill complexes in the Bangemall Supergroup, Western Australia: Geology, geochemistry, and mineralization potential: Geological Survey of Western Australia, Report 99, 75p.

Muhling, PC and Brakel, AT 1985, Geology of the Bangemall Group: The evolution of a Proterozoic intra-cratonic sedimentary basin: Geological Survey of Western Australia, Bulletin 128, 266p.

Nockolds, SR, Knox, RWO'B and Chinner, GA 1978, Petrology for students: Cambridge University Press, Cambridge, 440p.

Olierook, HKH, Plavsa, D, Reddy, SM, Yao, W, Clark, C, Occhipinti, SA and Kylander-Clark, ARC 2019, Neoproterozoic hydrothermal activity in the West Australian Craton related to Rodinia assembly or breakup? Gondwana Research, v. 68, p. 1–12, doi:10.1016/j.gr.2018.10.019.

Pang, C-J, Wang, X-C, Xu, B, Zhao, J-X, Feng, Y-X, Wang, Y-Y, Luo, Z-W and Liao, W 2016, Late Carboniferous N-MORB-type basalts in central Inner Mongolia, China: Products of hydrous melting in an intraplate setting? Lithos, v. 261, p. 55–71, doi:10.1016/j.lithos.2016.05.005.

Pearce, JA 1975, Basalt geochemistry used to investigate past tectonic environments on Cyprus: Tectonophysics, v. 25, no. 1–2, p. 41–67.

Pearce, JA 1996, A users guide to basalt discrimination diagrams, *in* Trace element geochemistry of volcanic rocks: applications for massive-sulphide exploration *edited by* DA Wyman: Geological Association of Canada, Short Course Notes, p. 79–113.

Pearce, JA 2008, Geochemical fingerprinting of oceanic basalts with applications to ophiolite classification and the search for Archean oceanic crust: Lithos, v. 100, p. 14–48.

Pearce, JA and Peate, DW 1995, Tectonic implications of the composition of volcanic arc magmas: Earth and Planetary Science Letters, v. 23, p. 251–285, doi:10.1146/annurev.ea.23.050195.001343.

Peng, P and Ernst, R 2016, Dyke swarms: Keys to paleogeographic reconstructions, preface for IDC7 2016, Bejing, China, 2016/08/18: Acta Geologica Sinica, v. 90, supp. 1, Abstracts of the Seventh International Dyke Conference, 'Dyke Swarms': Keys to Paleogeographic Reconstruction, 447p.

Piechocka, AM, Sheppard, S, Fitzsimons, ICW, Johnson, SP, Rasmussen, B and Jourdan, F 2018, Neoproterozoic 40Ar/39Ar mica ages mark the termination of a billion years of intraplate reworking in the Capricorn Orogen, Western Australia: Precambrian Research, v. 310, p. 391–406, doi:10.1016/j.precamres.2018.04.006.

Pirajno, F and Hoatson, DM 2012, A review of Australia's Large Igneous Provinces and associated mineral systems: Implications for mantle dynamics through geological time: Ore Geology Reviews, v. 48, p. 2–54.

Pirajno, F and Santosh, M 2015, Mantle plumes, supercontinents, intracontinental rifting and mineral systems: Precambrian Research, v. 259, p. 243–261, doi:10.1016/j.precamres.2014.12.016.

Rasmussen, B, Fletcher, IR and Sheppard, S 2005, Isotopic dating of the migration of a low-grade metamorphic front during orogenesis: Geology, v. 33, p. 773–776.

Rice, JM, Dickey, JS and Lyons, JB 1971, Skeletal crystallization of pseudobrookite: American Mineralogist, v. 56, no. 1–2, p. 158–162.

Rollinson, HR 1993, Using geochemical data: Evaluation, presentation, interpretation: Pearson Education Ltd, Harlow, England, 352p.

Sheppard, S 2004, Unravelling the complexity of the Gascoyne Complex, *in* GSWA 2004 extended abstracts: promoting the prospectivity of Western Australia: Geological Survey of Western Australia, Record 2004/5, p. 26–28.

Sheppard, S, Bodorkos, S, Johnson, SP, Wingate, MTD and Kirkland, CL 2010, The Paleoproterozoic Capricorn Orogeny: Intracontinental reworking not continent-continent collision: Geological Survey of Western Australia, Report 108, 33p.

Sheppard, S and Johnson, SP 2018, Pooranoo Metamorphics (P_-PO-md): WA Geology Online, Explanatory Notes extract: Geological Survey of Western Australia, accessed 22 August 2018, <www.dmirs.wa.gov.au/ens>.

Sheppard, S and Johnson, SP 2019, Leake Spring Metamorphics (P_-LS-xmd-mk): WA Geology Online, Explanatory Notes extract: Geological Survey of Western Australia, accessed 2 June 2020, <www.dmirs.wa.gov.au/ens>.

Sheppard, S, Johnson, SP, Korhonen, FJ and Occhipinti, SA 2018a, Durlacher Supersuite (P_-DU-g): WA Geology Online, Explanatory Notes extract: Geological Survey of Western Australia, accessed 22 August 2018, <www.dmirs.wa.gov.au/ens>.

Sheppard, S, Johnson, SP and Occhipinti, SA 2018b, Moorarie Supersuite (P_-MO-g): WA Geology Online, Explanatory Notes extract: Geological Survey of Western Australia, accessed 22 August 2018, <www.dmirs.wa.gov.au/ens>.

Sheppard, S, Rasmussen, B, Muhling, JR, Farrell, TR and Fletcher, IR 2007, Grenvillian-aged orogenesis in the Palaeoproterozoic Gascoyne Complex, Western Australia: 1030–950 Ma reworking of the Proterozoic Capricorn Orogen: Journal of Metamorphic Geology, v. 25, p. 477–494.

Smithies, RH, Kirkland, CL, Korhonen, FJ, Aitken, ARA, Howard, HM, Maier, WD, Wingate, MTD, Quentin de Gromard, R and Gessner, K 2015, The Mesoproterozoic thermal evolution of the Musgrave Province in central Australia — plume vs. the geological record: Gondwana Research, v. 27, no. 4, p. 1419–1429, doi:10.1016/j.gr.2013.12.014.

Srivastava, RK (editor) 2011, Dyke swarms: keys for geodynamic interpretation: Springer-Verlag, Berlin, 605p.

Stern, RA 2001, A new isotopic and trace element standard for the ion microprobe: preliminary thermal ionization mass spectrometry (TIMS) U–Pb and electron-microprobe data: Resources naturelles, Canada.

Sun, S-S and McDonough, WF 1989, Chemical and isotopic systematics of oceanic basalts: implications for mantle composition and processes, *in* Magmatism in the Ocean Basins *edited by* AD Saunders and MJ Norry: Geological Society, London, Special Publication 42, p. 313–345.

Tarney, J (editor) 2011, Dyke swarms: keys for geodynamic interpretation: 6th International Dyke Conference: Springer-Verlag Science, Berlin, 605p.

Thorne, AM 2015, Bresnahan Group (P_-BR-s): WA Geology Online, Explanatory Notes extract: Geological Survey of Western Australia, accessed 2 June 2020, <www.dmirs.wa.gov.au/ens>.

Thorne, AM 2016a, Collier Group (P_-MS-s): WA Geology Online, Explanatory Notes extract: Geological Survey of Western Australia, accessed 8 December 2017, <www.dmirs.wa.gov.au/ens>.

Thorne, AM 2016b, Edmund Group (P_-ME-xs-k): Geological Survey of Western Australia, accessed 6 December 2017, <www.dmirs.wa.gov.au/ens>.

Thorne, AM 2018a, Ashburton Basin (AS): WA Geology Online, Explanatory Notes extract: Geological Survey of Western Australia, accessed 22 August 2018, <www.dmirs.wa.gov.au/ens>.

Thorne, AM 2018b, Blair Basin (BL): WA Geology Online, Explanatory Notes extract: Geological Survey of Western Australia, accessed 22 August 2018, <www.dmirs.wa.gov.au/ens>.

Thorne, AM 2018c, Gooragoora Formation (P_-MEg-ss): WA Geology Online, Explanatory Notes extract: Geological Survey of Western Australia, accessed 3 June 2020, <www.dmirs.wa.gov.au/ens>.

Thorne, AM 2018d, Ullawarra Formation (P_-MEl-sl): WA Geology Online, Explanatory Notes extract: Geological Survey of Western Australia, accessed 22 May 2019, <www.dmirs.wa.gov.au/ens>.

Thorne, AM 2020, Wyloo Group (P_-WY-s): WA Geology Online, Explanatory Notes extract: Geological Survey of Western Australia, accessed 2 June 2020, <www.dmirs.wa.gov.au/ens>.

Thorne, AM and Cutten, HN 2010, Tangadee, WA Sheet 2649: Geological Survey of Western Australia, 1:100 000 Geological Series.

Thorne, AM and Johnson, SP 2018, Capricorn Group (P_-CP-sk): WA Geology Online, Explanatory Notes extract: Geological Survey of Western Australia, accessed 2 June 2020, <www.dmirs.wa.gov.au/ens>.

Thorne, AM and Martin, DMcB 2007, Peedawarra, WA Sheet 2349: Geological Survey of Western Australia, 1:100 000 Geological Series.

Thorne, AM, Martin, DMcB and Copp, IA 2004, Capricorn, WA Sheet 2251: Geological Survey of Western Australia, 1:100 000 Geological Series.

Vernon, RH 1983, Restite, xenoliths and microgranitoid enclaves in granites: Journal of the Proceedings of the Royal Society of New South Wales, v. 116, p. 77–103.

Wang, Q 2013, Geochronology of the granite–greenstone terranes in the Murchison and Southern Cross Provinces of the Yilgarn Craton, Western Australia: The Australian National University, doi: 10.25911/5d78d8c207fb1.

Wang, X-C, Li, Z-X, Li, J, Pisarevsky, SA and Wingate, MTD 2014, Genesis of the 1.21 Ga Marnda Moorn large igneous province by plume-lithosphere interaction: Precambrian Research, v. 241, p. 85–103.

Winchester, JA and Floyd, PA 1976, Geochemical magma type discrimination: Application to altered and metamorphosed basic igneous rocks: Earth and Planetary Science Letters, v. 28, no. 3, p. 459–469.

Wingate, MTD 2002, Age and palaeomagnetism of dolerite sills of the Bangemall Supergroup on the Edmund 1:250 000 sheet: Geological Survey of Western Australia, Record 2002/4, 48p.

Wingate, MTD 2003, Age and palaeomagnetism of dolerite intrusions of the southeast Collier Basin and the Earaheedy and Yerrida Basins, Western Australia: Geological Survey of Western Australia, Record 2003/3, 34p.

Wingate, MTD 2017a, Mafic dyke swarms and large igneous provinces in Western Australia get a digital makeover, *in* GSWA 2017 Extended abstracts: promoting the prospectivity of Western Australia: Geological Survey of Western Australia, Record 2017/2, p. 4–8.

Wingate, MTD and Blay, OA 2020, Mundine Well Dolerite (P_-_mw-od): WA Geology Online, Explanatory Notes extract: Geological Survey of Western Australia, accessed 20 July 2018, <www.dmirs.wa.gov.au/ens>.

Wingate, MTD and Giddings, JW 2000, Age and palaeomagnetism of the Mundine Well dyke swarm, Western Australia: Implications for an Australia-Laurentia connection at 755 Ma: Precambrian Research, v. 100, p. 335–357.

Wingate, MTD, Kirkland, CL and Cutten, HN 2012, 143440: felsic metavolcaniclastic rock, Nicken Bore; Geochronology Record 1029: Geological Survey of Western Australia, 6p.

Wingate, MTD, Kirkland, CL, Thorne, AM and Cutten, HN 2014, 189219: siltstone, ESR Well No.12; Geochronology Record 1210: Geological Survey of Western Australia, 5p.

Wingate, MTD and Lu, Y 2018, Introduction to geochronology information: Geological Survey of Western Australia, 5p.

Wingate, MTD, Lu, Y, Blay, O and Johnson, SP 2017b, 206949: dolerite dyke, Tin Hut Bore; Geochronology Record 1431: Geological Survey of Western Australia, 4p.

Wingate, MTD, Lu, Y, Blay, O and Johnson, SP 2017c, 206949: dolerite dyke, Tin Hut Bore; Geochronology Record 1432: Geological Survey of Western Australia, 4p.

Wingate, MTD, Pirajno, F and Morris, PA 2004, Warakurna large igneous province: A new Mesoproterozoic large igneous province in west-central Australia: Geology, v. 32, no. 2, p. 105–108.

Zhao, JX, McCulloch, MT and Korsch, RJ 1994, Characterisation of a plume-related ~800 Ma magmatic event and its implications for basin formation in central-southern Australia: Earth and Planetary Science Letters, v. 121, no. 3-4, p. 349–367, doi:10.1016/0012-821X(94)90077-9.

RECORD 2020/12

PROTEROZOIC DOLERITE DYKES IN THE WESTERN CAPRICORN OROGEN, WESTERN AUSTRALIA

Blay et al.

This Record is published in digital format (PDF) and is available as a free download from the DMIRS website at <www.dmirs.wa.gov.au/GSWApublications>.

Further details of geoscience products are available from:

Information Centre
Department of Mines, Industry Regulation and Safety
100 Plain Street
EAST PERTH WESTERN AUSTRALIA 6004
Phone: +61 8 9222 3459 Email: publications@dmirs.wa.gov.au
www.dmirs.wa.gov.au/GSWApublications